GNSS time series and velocities about a slowly convergent margin processed on HPC clusters: products and robustness evaluation

Lavinia Tunini[1], Andrea Magrin[1], Giuliana Rossi[1], David Zuliani[1]

[1]National Institute of Oceanography and Applied Geophysics - OGS, Trieste-Udine, Italy

Correspondence to: Lavinia Tunini (ltunini@ogs.it)

Abstract. Global Navigation Satellite Systems are well-known and fundamental tools for crustal monitoring projects and tectonic studies, thanks to their high coverage and the high-quality of the data they provide. In particular, at slowly convergent margins, where deformation rates are of the order of a few mm/yr, GNSS monitoring proves to be beneficial in detecting the diffuse deformation responsible for tectonic stress accrual. Its strength lies in the high precision achieved by GNSS permanent stations, especially when long-term data and stable monuments are available at the stations. North-East Italy is a tectonically active region located in the northernmost sector of the Adria microplate, slowly converging with the Eurasia plate, characterised by low deformation rates and moderate seismicity. It greatly benefits from continuous and high-precision geodetic monitoring, since it has been equipped with a permanent GNSS network providing real-time data and daily observations over two decades. The Friuli Venezia Giulia Deformation Network (FReDNet) was established in the area in 2002 to monitor crustal deformation and contribute to the regional seismic hazard assessment. This paper describes GNSS time series spanning two decades of stations located in the NE-Italy and surroundings, as well as the outcoming velocity field. The documented dataset has been retrieved by processing the GNSS observations with the GAMIT/GLOBK software ver10.71, which allows calculating high-precision coordinate time series, position and velocity for each GNSS station, and by taking advantage of the high-performance computing resources of the Italian High-Performance Computing Centre (CINECA) clusters.

The GNSS observations (raw and standard RINEX formats) and the time series estimated with the same procedure are currently daily continued, collected and stored in the framework of a long-term monitoring project. Instead, velocity solutions are planned to be updated annually. The time series and velocity field dataset documented here is available on Zenodo (https://doi.org/10.5281/zenodo.8055800, Tunini et al., 2024).

1 Introduction

The Global Navigation Satellite System (GNSS) allows obtaining a globally-extended positioning dataset which is essential not only for crustal deformation and tectonic studies but also for plenty of applications going from surveying to metrology and hazard monitoring projects in the environmental sciences. In recent years, the GNSS system has been continuously and rapidly growing, with multi-constellation and multi-frequency signals supported by cutting-edge processing algorithms

1

31 devoted to the integration of different sensors (sensor fusion techniques) and improvements in error mitigation procedures.

32 The well-known GPS, combined with GLONASS and the more recent Galileo and Beidou constellations, can provide velocity

33 estimates of the GNSS stations with precisions less than 1 mm/yr when long time-series, precise satellite orbits, and stable

34 monuments are available at the stations.

35

Fig. 1: Map of the study area, with topography from ETOPO1 (Amante and Eakins, 2009). Red lines indicate the boundary of the Adria microplate; we refer to the "Adria microplate" as the Adriatic sea plate domain, also including the Apulia block in the southern Adriatic sea. Continental lithosphere polygons from GPlates 2.1 dataset (https://www.earthbyte.org/gplates-2-1-software-and-data-sets/) are in agreement with Matthews et al. (2016). AL: Albania; AS: Adriatic Sea; AU: Austria; CR: Croatia; EA: Eastern Alps; NEI: North-East Italy; SL: Slovenia.

41

Notwithstanding the availability of reliable and consistent GNSS solutions at the global scale, such as those provided by the Nevada Geodetic Laboratory (NGL) (http://geodesy.unr.edu/; Blewitt et al., 2018), at the regional scale, it may be useful to consider an ad hoc reference frame and to customise the processing scheme, in order to obtain high-quality time series and high-quality velocity field in regions of particular interest. North-East Italy (Fig. 1) is a particularly suitable region, because of the large number of GNSS stations deployed there by different agencies since the early 2000s to monitor the deformations. North-East Italy lies at the northern edge of the Adria microplate, a continental lithosphere block, part of the distributed deformation zone between the African and Eurasian plates, encompassing the eastern Italian peninsula from Sicily to the border with Austria and Slovenia, and the eastern Adriatic coast from Slovenia to Croatia and Albania (Battaglia et al., 2003). Adria microplate is recognized to have a counterclockwise motion, implying its collision with Eurasia along its northern tip (Battaglia et al., 2003; D'Agostino et al., 2005, 2008; Serpelloni et al., 2005). The convergence between Adria and Eurasia plates leads to significant consequences on the deformation of the NE-Italy, as revealed by the moderate seismicity, primarily concentrated in the southern sector of the Eastern Alps, and diffused tectonic deformation (Castellarin and Cantelli, 2000; Bressan et al., 2021). Although the deformation rates (2–3 mm/yr of N-S shortening; D'Agostino et al., 2005; Weber et al., 2010; Devoti et al., 2011) remain quite low if compared to fast converging margins like India-Eurasia or Arabia-Eurasia, this is the most seismic active area of the entire Alps chain. Hence, northeastern Italy is a key region for the understanding of the Adria Plate geodynamics (Brancolini et al., 2019; Magrin and Rossi, 2020). The deformation in the area is currently monitored through GNSS instruments by the National Institute of Oceanography and Applied Geophysics - OGS, the Friuli Venezia Giulia regional council and other entities, providing new and denser data to the information available since the 60s of the 20th century from the NE-Italy subsurface tilt and strainmeter network (Braitenberg and Zadro, 1999, Rossi et al., 2021). The Friuli Venezia Giulia Deformation Network (FReDNet) is the GNSS network established by the OGS to monitor the distribution of the crustal deformation and provide supplementary information for the regional earthquake hazard assessment (Zuliani et al., 2018). It currently includes 22 permanent GNSS stations located at distances of 15-20 km from each other in most parts of the region, most of which have been in operation for more than 15 years (more details in Appendix A). FReDNet is part of the OGS seismic and geodetic monitoring system for the North-East Italy (Sistema di Monitoraggio terrestre dell'Italia Nord Orientale - SMINO), which also includes seismic broad-band and short and mean period stations, as well as strong motion stations (Bragato et al., 2021 and references therein).

In this paper, we document a dataset of position time series and velocities for 350 stations in NE-Italy and surroundings, whose data have been continuously collected over the past two decades. The dataset has the potential to provide high-quality and updated information relative to an active but slow converging margin. Data have been processed taking advantage of the high-performance computing resources offered by CINECA (https://www.hpc.cineca.it/) clusters through the Italian SuperComputing Resource Allocation - ISCRA initiative, and through the resources available inside the HPC Training and Research for Earth Sciences (HPC-TRES) program, co-sponsored by the Minister of Education, University and Research (MIUR). The HPC-TRES training program, drown-up by OGS and CINECA, is targeted to promote advanced training in the

75 fields of Earth System sciences and enhance human resources and capacity building through the use of national and European

76 HPC infrastructures and services in the framework of the international infrastructure PRACE - The Partnership for Advanced

77 Computing in Europe (https://prace-ri.eu/). In Section 2 and in Section 3, we describe the collected input data and the

78 elaboration procedures, respectively. The dataset of time series and velocities is presented in Section 4, whereas Section 5

79 illustrates some experiments to evaluate the dataset's quality and robustness. Section 6 provides information on the data

80 availability and Section 7 outlines some final considerations.

81

2 Input data

83 We considered the data recorded by all available permanent GNSS stations located in North-East Italy and surrounding

84 regions (Fig. 2). These stations belong to different networks: the OGS geodetic network FReDNet (http://frednet.crs.ogs.it/);

85 the GNSS network Antonio Marussi of the Friuli Venezia Giulia (FVG) regional council (Marussi), with stations located

86 throughout the FVG region, that enhance the coverage offered by FReDNet; the Veneto region GPS network (VNTO); the

87 Servizio di Posizionamento SPIN3 GNSS (SPIN), which is a network covering Lombardia, Piemonte and Valle D'Aosta

88 regions; the South Tyrolean Positioning Service (STPOS) and Trentino POsitioning Service (TPOS), which are the geodetic

89 networks of the Autonomous Provinces of Trento and Bolzano, respectively; the Liguria region GNSS network (LIGU); the

90 Rete Nazionale Integrata GNSS (RING) belonging to the National Institute of Geophysics and Volcanology (INGV); the

91 Nuova Rete Fiduciale Nazionale GNSS of the Italian Space Agency (ASI); the European EUREF Permanent Network (EPN),

92 which includes stations managed by different institutions; the Echtzeit Positionierung Austria (EPOSA) network; the

93 SIGNAL network of the Geodetic Institute of Slovenia (SIGN) and other Slovenian GNSS stations acquired by OGS in

94 agreement with the University of Ljubljana and the non-profit organisation Zavod MPRI, raziskovalna in razvojna dejavnost

95 (previously with the Slovenian company Harphasea) (in the following: SLO_GPS). More details can be found in Appendix

96 B. Although some of these networks were designed for cadastral and civil purposes, the validity of such data for velocity

97 estimates has been demonstrated in several works since the benefit of redundancy and increased spatial density overcomes

98 the noise eventually present (Serpelloni et al., 2022 and references therein).

99

100
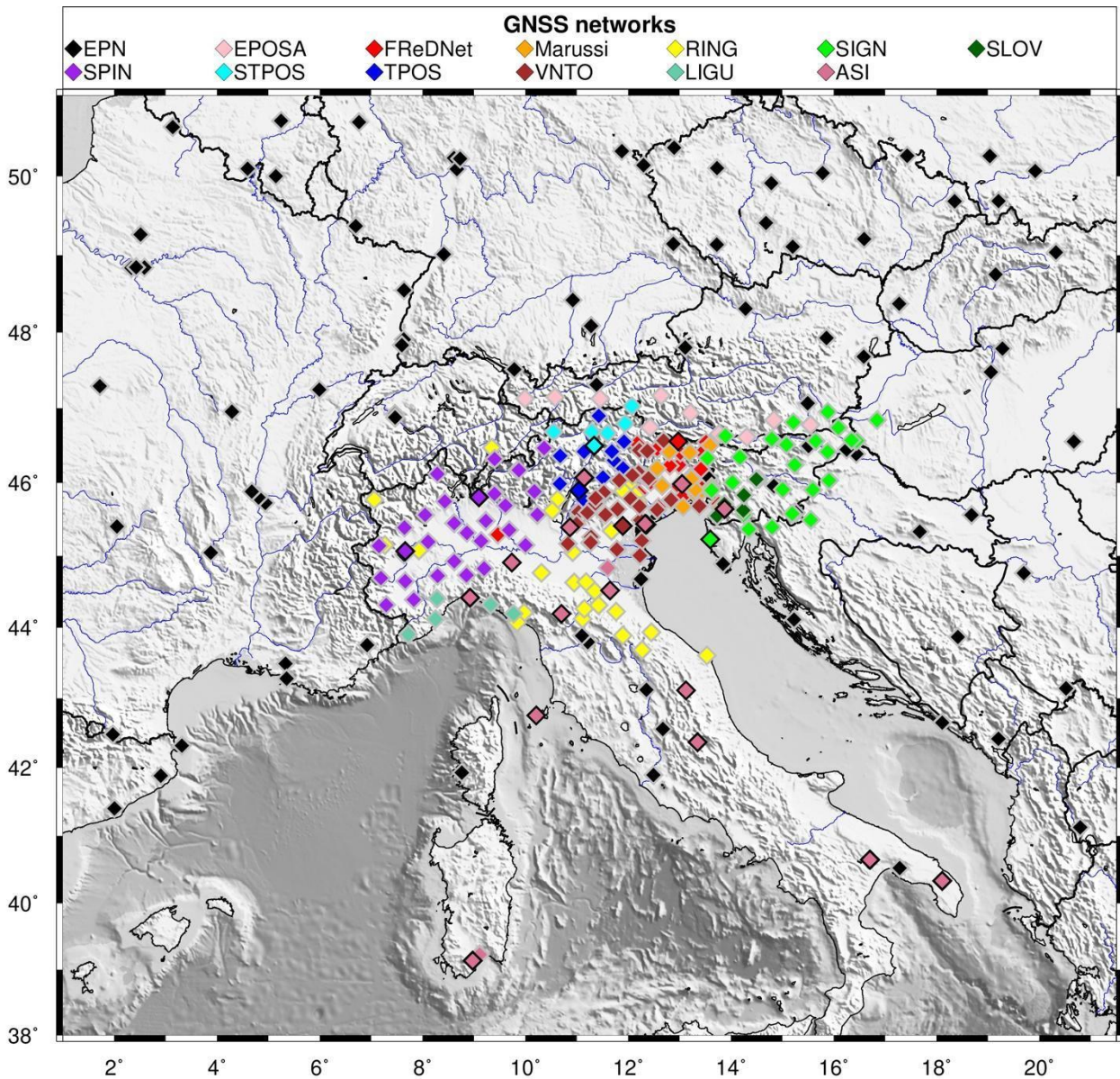
Fig 2: GNSS stations location and belonging networks. Different colours stand for different networks, as indicated in the legend (see main text for the abbreviations). Symbols contoured by black lines indicate those stations belonging to both a regional network and to the European network EPN.

104

In order to link our solutions to the International Terrestrial Reference Frame ITRF14 (Altamimi et al., 2016), we also consider

the data coming from reference sites belonging to the EPN and the International GNSS Service (IGS, https://igs.org/data/)

networks. In a rectangular area extending from 39.75°N to 50.70°N latitude and from 1.5° to 21°E longitude and centred in

108   N-E Italy, whose size has been empirically selected to obtain a stable position-velocity solution for each of the target stations,

109   we consider as reference sites all the EPN and IGS sites located inside it, with four additional EPN sites located in Sardinia

110   (CAGL, CAG1, CAGZ and UCAG) added to improve the coverage in the southern sector. While our study encompasses

111   more than 350 stations within the designated area (5 stations - GUMM, LECC, LEIB, RUDI, SILL - were moved more than

112   1 m from the original position; therefore, we renamed them), the actual volume of data is considerably lower. It has shown a

113   progressive increase, starting from just a few tens of data per day in 2002, to reaching approximately 250 data points per day

114   in 2011 (Fig. 3). The drop in the number of stations since 2013 is due to a sudden restriction of the access to several stations

115   located in Slovenia. The data availability highly depends on station operability, remote connection functioning, and

116   decommissioning/installation of stations.

117   The total number of the daily observation files processed in this study is about 0.57 million.

118
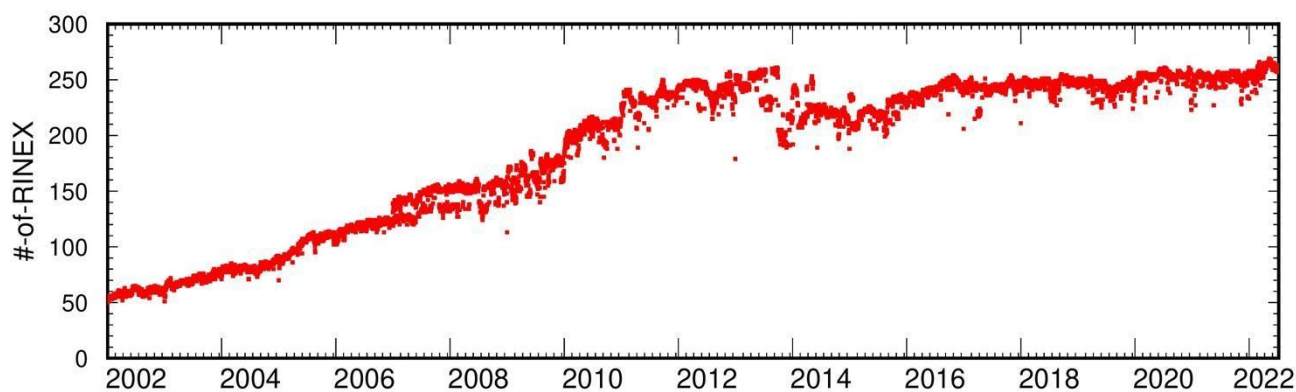
119

120   **Fig. 3: Amount of data available with time.**

121

122   We have collected GNSS observation data since 2002, 1st January. Raw data from the FReDNet network are collected,

123   quality-checked, transformed into the Receiver INdependent EXchange (RINEX) format, and then released, through a public

124   ftp repository, as hourly and daily files at both 1s and 30s sampling. Data from EPOSA network and SLO_GPS stations are

125   collected in real-time through the GNSMART software (Gerhard et al., 2001) and then converted into RINEX format for

126   post-processing. Finally, RINEX-formatted data deriving from the other networks are collected using different services of

127   data distribution: public data repository of the networks, EPN data distribution services and European Plate Observation

128   System (EPOS) service (Fig. 4).

129   Like the SMINO monitoring system to which it belongs, the FReDNet network aims to provide a monitoring service on a

130   long-term basis. Hence, raw observations and RINEX-formatted data from FReDNet stations are currently continuously

131   retrieved, collected and stored in the OGS internal repository on hourly and daily basis (https://doi.org/10.6092/frednet, OGS,

132   2016), where also real-time observations are available. FReDNet data are distributed under a Creative Common licence (CC

6

133   BY 4.0) and accessible at the link https://doi.org/10.6092/frednet. They are allocated into folders according to the sampling

134   interval and to the date of the acquisition. From the same web page metadata of FReDNet stations are also retrievable by

135   clicking on the "sitelogs" link.

136
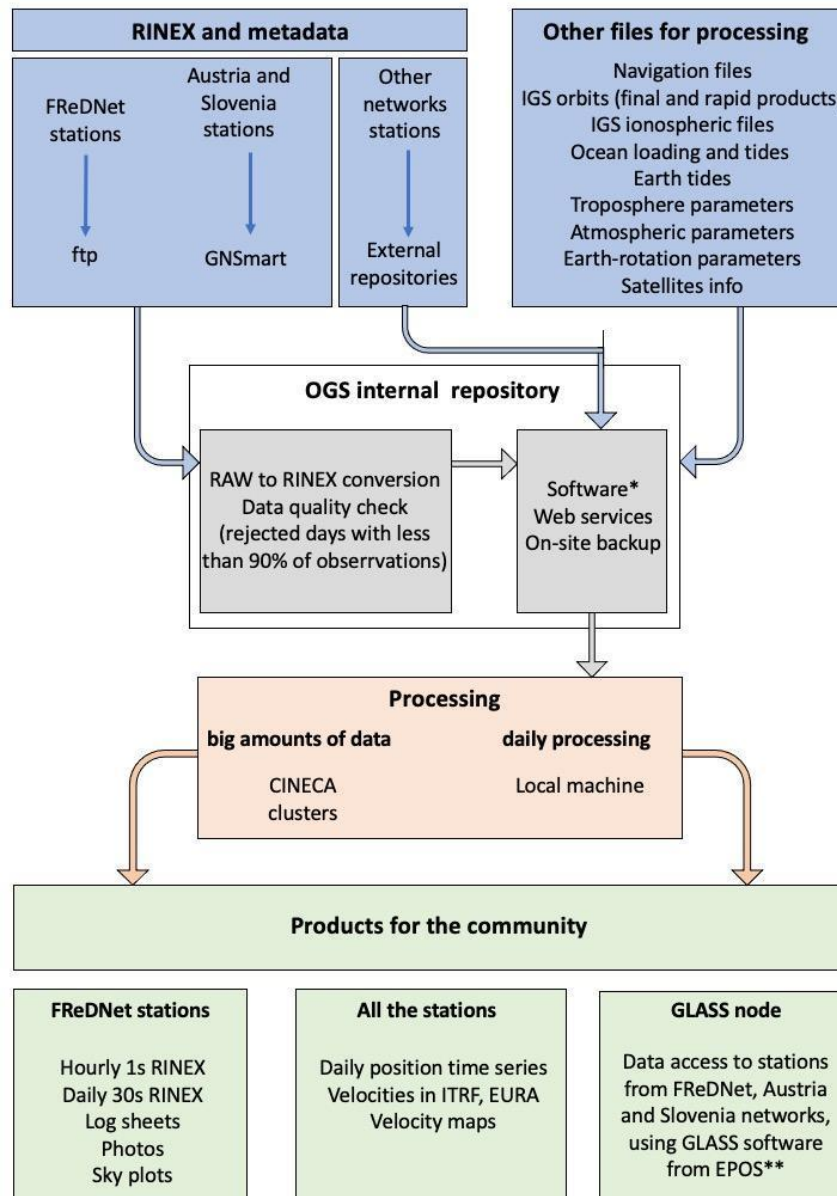
137

138   **Fig. 4: GNSS data flow at the OGS (Italy). *Software used: GAMIT/GLOBK ver10.71 (Herring et al., 2018) for GNSS data**
139   **processing, GMT ver6.4.0 for plots and maps, GNSMART for downloading raw streams data from Austria and Slovenia networks**
140   **and transform them into RINEX format data, TEQC (Estey and Meertens, 1999) for data quality check (it is end-of-life, but for**
141   **GPS data it is still functional), Git ver2.27, free and open source system (https://git-scm.com/), for scripts updating and management**

142 **between different machines, Anubis ver2.3 (https://gnutsoftware.com/software/anubis) for sky plots and RINEX3 generation. ****
143 **https://glass.gnss-epos.eu/#/site**

145 Along with the data, sitelogs containing station metadata (e.g. station location, monument type, terrain description, photos,
146 etc.) are collected for each GNSS station. The primary information source for metadata are the log sheets in IGS format
147 (https://www.igs.org/formats-and-standards/) recovered through the public repository of each networks and from the
148 "Metadata Management and distribution system for Multiple GNSS Networks" (M3G) (https://gnss-metadata.eu/site/index).
149 If the network does not provide IGS sitelogs, we extract the information from RINEX files header. Finally, we verify the
150 compatibility among different sources of metadata, when available.

151 Metadata describes the history of the equipment, which is useful for classifying discontinuities in the time series. We use this
152 information to populate the list of offsets in the time series for the stations' a priori coordinates. In particular, we define the
153 offsets present in the time series by considering (i) the sitelog information on station equipment; (ii) the offsets reported by
154 EUREF and IGS, except those related to changes in the processing procedure; (iii) the occurrence of earthquakes with
155 magnitude greater than 5.0 as reported by ANSS catalogue (U.S.G.S., 2017), with an offset assigned to each station within
156 an empirical radius of influence as a function of the magnitude (using the *sh_makeeqdef* program inside the GAMIT/GLOBK
157 software, Herring et al., 2018).

158 Another important information reported in the sitelog of a GNSS station concerns the monument type and its location (on a
159 building roof, on a building wall, or on the ground). The monument for a GPS/GNSS site should be designed to provide stable
160 and secure support to mount the antenna. Therefore the monument should comply with a certain number of characteristics.
161 The IGS and University NAVSTAR Consortium (UNAVCO) provide some recommendations for the monumentation and
162 the installation site (https://files.igs.org/pub/station/general/IGS%20Site%20Guidelines%20July%202015.pdf,
163 https://kb.unavco.org/article/unavco-resources-permanent-gps-gnss-stations-634.html). It is not always easy to accomplish
164 all these requirements, because it is difficult to cover all the conditions and because the same environment changes over time,
165 especially near urban areas, due to urban developments. The consequences of non-optimal site conditions are likely to be
166 reflected in data quality, noisy time series, and increased uncertainties.
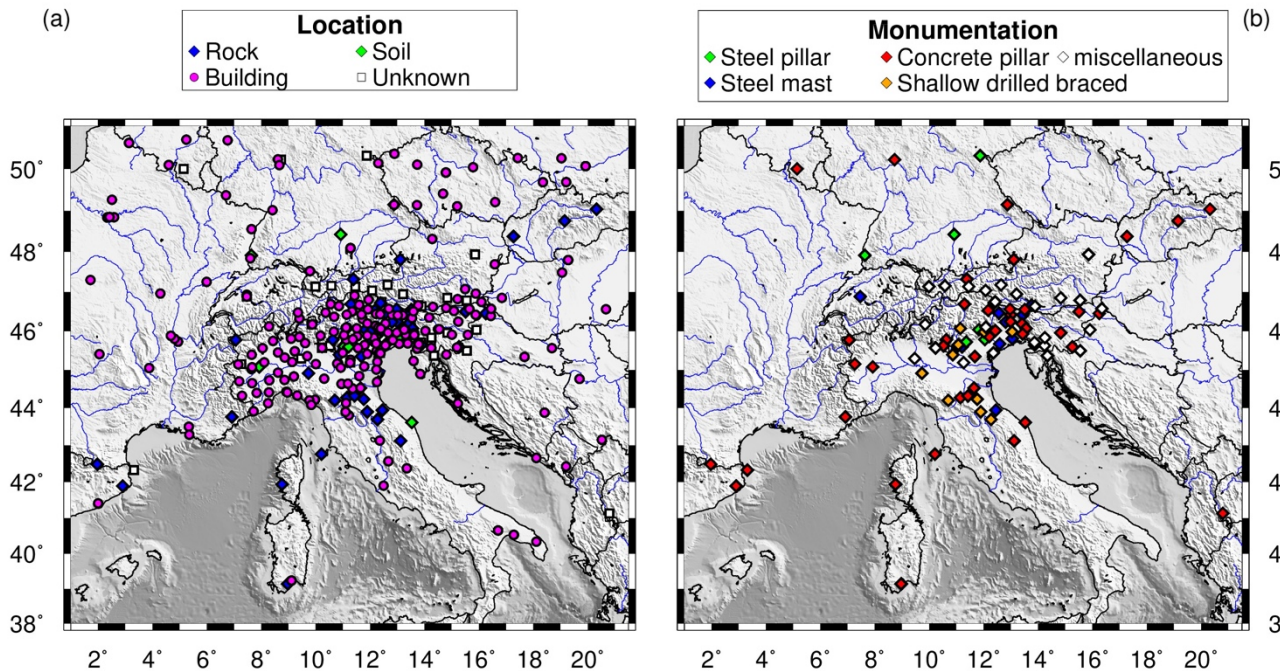
Fig. 5: Information on the location and monument type of the GNSS stations considered in this study. a) Stations classified according to their location. Rock = station installed on hard terrain (not soil) or outcropping rocks. Building = station installed on a building or similar manufacts, like a wall, both on roof or fixed to the side wall. Soil = station installed on a soft terrain. Unknown = station whose location description is incomplete or ambiguous. b) Stations not on buildings classified according to monument type. Steel pillar = monument made by a steel column. Steel mast = monument made by a steel bar. Concrete pillar = monument made by a concrete column with or without steel bars inside. Shallow drilled braced = monument consisting of a tripod drilled in the terrain). Miscellaneous includes mixed or not specified material.

The sitelog of a GNSS site should provide a detailed description of the monument (material type, monument foundation, high and depth of the foundation, geological characteristics of the bedrock, spacing of eventual fractures in the bedrock, presence of faults nearby) accompanied by a photograph of the same. However, sitelogs are often incomplete and lack images. Figure 5 shows the monument information retrieved from the sitelogs of our stations. Hence, we classify as anonymous the monument locations whose description in the sitelog is incomplete or ambiguous, and no photos or other sources of information are available to verify the data (Fig. 5a).

For the stations installed on the roof or the wall of a building, we can reasonably assume that the stability is more affected by the edifice, than by the monument's composition (a steel mast or a concrete pillar). Therefore, we classify only the stations located away from buildings according to the monument material (Fig. 5b).

As can be noticed from the figure, the majority of stations are located on buildings/walls (251), and just one-third (107) of stations are located in the free-field (10 on soft soil, 57 on exposed rocks, and 40 are on unknown free-field locations). Approximately 50% of the latter have concrete pillars as monuments (54), ~10% have a monument composed of steel rods

9

189 or a steel tripod (shallow drilled braced, http://ring.gm.ingv.it/?page_id=43) (11), while the rest of the stations have steel mast

190 monuments (9), steel pillar equipped stations (6) or not defined monument types (27).

191 **3 Data processing**

192 We process the GPS data using the GAMIT/GLOBK software package (ver 10.71) (Herring et al., 2018). GAMIT can estimate

193 station positions, atmospheric delays, satellite orbits, and Earth Orientation Parameters (EOP) from ionosphere-free linear

194 combination of GNSS phase observables, by using the double-differencing technique to eliminate phase biases caused by

195 drifts in the satellite and receiver clock oscillators. It outputs loosely constrained solutions (h-files) of the parameter estimates

196 and their covariance matrix. GLOBK is a module which implements the Kalman filtering, and it is used to combine the loosely

197 constrained solutions (between networks and through time) and to constrain the results into a consistent reference frame.

198 We process the data following these steps:

199 - definition of the sub-networks (subsets of stations);

200 - computation of the loosely constrain solutions for each sub-network;

201 - combination of the sub-networks solutions and computation of the daily position for each station;

202 - computation of the GNSS station velocities.

203 The RINEX files available each day are processed after being divided into subnetworks to pursue computational efficiency.

204 To do that, we use the *netsel* program of the GAMIT/GLOBK software package, which considers the geographic distribution

205 of the stations in order to build the subnetworks (see Serpelloni et al., 2022 for a detailed description of the algorithm). Each

206 subnetwork is linked to the next one by one station. An additional sub-network that contains two tie sites from each sub-

207 network links all the sub-networks together. We perform some tests to identify the best nominal number of stations for each

208 subnetwork, which depends on the amount of data available: we select 30 stations/subnetwork until 2008 and 40

209 stations/subnetwork for the following years. Stations from SLO_GPS network are equipped with receivers, whose data need

210 to be elaborated using the LC_HELP algorithm of the GAMIT/GLOBK software, which uses ionospheric constraints. To

211 include these stations in the solution, we process them in a separate sub-network along with some tie sites (TRIE, GSR1 and

212 KDA2). The tie sites of this sub-network will be excluded from *netsel* site list and added to the tie sites sub-network

213 afterwards.

214 We compute the loosely constrained solutions using the GAMIT module. GPS phase data are weighted according to an

215 elevation-angle-dependent error model (Herring et al., 2018) using an iterative analysis procedure whereby the elevation

216 dependence is determined by the observed scatter of phase residuals. Satellite precise orbits are retrieved from IGS repository

217 (http://www.igs.org/products/, Johnston et al., 2017). The first-order ionospheric delay is eliminated by using the ionosphere-

218 free linear combination for all the stations except the SLO_GPS ones. Further details about models and parameters are

219 reported in Table 1.

220

221

222   **Table 1: GAMIT solution parameters.**

Parameter	
Processing mode	Baseline - orbits parameters are not estimated
Elevation cutoff	10°
Precise orbits	IGS final products in SP3 format (https://www.igs.org/products/#orbits_clocks)
Broadcast Ephemeris data	RINEX navigation files from the Scripps Orbit and Permanent Array Center (SOPAC, http://sopac-csrc.ucsd.edu/) or from the Crustal Dynamics Data Information (http://cddis.nasa.gov, Noll, 2010)
Magnetic field	IGRF13 (Alken et al., 2021)
Ionospheric model	2nd-order ionosphere corrected through IGS IONEX files
Earth Orientation Parameters (pole position and UT1 and their rates of change)	Tightly constrained to *a priori* values obtained from IERS Bulletin A
Earth Rotation Model	IERS 2010 (Petit and Luzum, 2010)
Solid Earth tides	IERS 2010 (Petit and Luzum, 2010)
Ocean tidal loading	FES2004 (Lyard et al., 2006)
Atmospheric non tidal loading	Not applied
Atmospheric tidal loading	Not applied
A priori atmospheric parameters (pressure, temperature, zenith delay)	VMF1 grid (Vienna Mapping Function 1, Boehm et al., 2006)
Zenith delay estimation	estimates at 2-hr intervals for a 24hr session using a piecewise-linear (PWL) function
Tropospheric mapping function	VMF1 grid (Vienna Mapping Function 1, Boehm et al., 2006)

223

224

To obtain the position time series, we use the GLOBK module to combine the daily loosely constrained solutions of the subnetworks in a single daily solution leaving the constraints free. Since we want to express the solutions in the International Terrestrial Reference Frame (ITRF14/IGS14 by Altamimi et al., 2016; in particular, we use the newer GNSS geodetic reference frame IGb14), we then apply generalised constraints (Dong et al., 1998) using the *glorg* program. For this purpose, we use a six-parameter Helmert transformation (translation and rotation) estimated by minimising the difference in the positions of a set of stations with well-defined coordinates and velocities (reference sites) as a priori coordinates. We do not explicitly use scale to avoid potential absorption of height signals, following Herring et al. (2016). The results are daily position estimates for each station consistent with the IGb14 reference frame.

The time series are visually inspected to identify offsets that are not due to equipment changes or earthquakes. We automatically remove outliers using two criteria similar to those used by Floyd et al. (2010). First, we remove the daily positions that have formal uncertainty greater than 20 mm. Then we fit the time series to a model consisting of a linear trend and offsets through a weighted linear regression by using the *tsfit* program. The positions with residuals greater than three times the weighted root-mean-square (RMS) value of the fit are also removed. Finally, by applying the *real_sigma* algorithm (Floyd and Herring, 2019), which allows accounting for temporal correlations in the data, we estimate random walk values for each station from the analysis of the outlier-adjusted time series and identify specific sites exhibiting a random walk noise level exceeding 2.0 mm2/yr level, which are also removed.

To compute the velocity field, we use the forward-running Kalman filter implemented in the GLOBK module, in which the state vector includes the positions and velocities for each station (Herring et al., 2016). The input data are the daily loosely constrained solutions, as they may be freely rotated and translated, thus eliminating the need to include EOP in the state vector, and their full variance-covariance matrices. Following Herring et al. (2016), from the analysis of the previously generated time series, we retrieve the list of outliers to be excluded from the computation and the site specific parameters to model the stochastic noise on the station positions. At each epoch, the Kalman filter updates positions and velocities. With the aim of reducing the computation time, we divide the stations into sub-networks using *netsel*. We use a nominal number of 90 stations for each sub-network and the noise model obtained from the time series analysis. First, we estimated the velocities and positions of the stations included in each sub-network. Then, we combine the solutions obtained for each sub-network in a single solution. At the end of the forward Kalman filter run, we align positions and velocities to the IGb14 reference frame using twelve parameters Helmert transformation (rotation, translation and their rates). Velocities of stations within 1 km distance (including differently named stations at the same location) are equated in this reference frame realisation. Finally, we recalculate the time series and velocities using the values obtained in the previous iteration as *a priori* coordinates and expand the list of reference stations to include all the stations with random walk values lower than 0.5 mm2/yr. As reported by Herring et al. (2018), the time series that best represent the final velocity solution are those computed considering all stations in the solution as reference sites. We also express our solutions relative to the Eurasia plate as defined by Altamimi et al. (2017) plate motion model (ETRF14 reference frame) using the same procedure adopted for IGb14.

3.1 Computing infrastructure

Modern computational infrastructures allow the analysis of huge amounts of data with extraordinary advantages in terms of operational cost for data storage, processing and time-saving, leading to the timely provision of homogeneous products. We exploited the CINECA (https://www.hpc.cineca.it/) High-Performance Computing (HPC) resources to process and analyse in a very short time all the GNSS data available in the study area between 2002, January 1st and 2022, June 30th. We used the GALILEO100 Cluster, which is equipped with 554 compute nodes with 2 x CPU Intel CascadeLake 8260 each with 24 cores, 2.4 GHz, 384GB RAM DDR4. The job scheduling and workload management system is SLURM 21.08 (https://wiki.fysik.dtu.dk/niflheim/SLURM). SLURM is designed to accomplish three key functions: (i) allocation of exclusive/non-exclusive access to computing nodes to users for a specific duration of time; (ii) provision of a framework for managing the work (starting, execution, monitoring) on the set of allocated nodes; (iii) resources distribution handling by managing a queue of pending jobs.

Figure 6 is intended to give an indication of the performance of CINECA clusters for GNSS data elaborations showing the computation time on GALILEO100 computing nodes to obtain the GAMIT solutions as a function of the number of stations considered on each job sent to the compute nodes. The figure shows that the computation time varies on average with the square of the number of stations. Although the calculations of the GAMIT solutions are the most time-consuming jobs of the processing procedure, the total computation time on GALILEO100 depends not only on the number of available daily data but also on the adopted parallelization strategy (i.e., the number of jobs sent to resources on compute nodes) and the occupancy of the machine (i.e., queue waiting time). In our study, we managed to process two decades of GNSS data in one week. We implemented the same procedure described in the previous section on a local machine to process the data daily following the 30th of June 2022, with the aim of keeping the products updated. The daily processing is automated by using the crontab utility. More details on the implementation on the local machine can be found in the Appendix C.

281
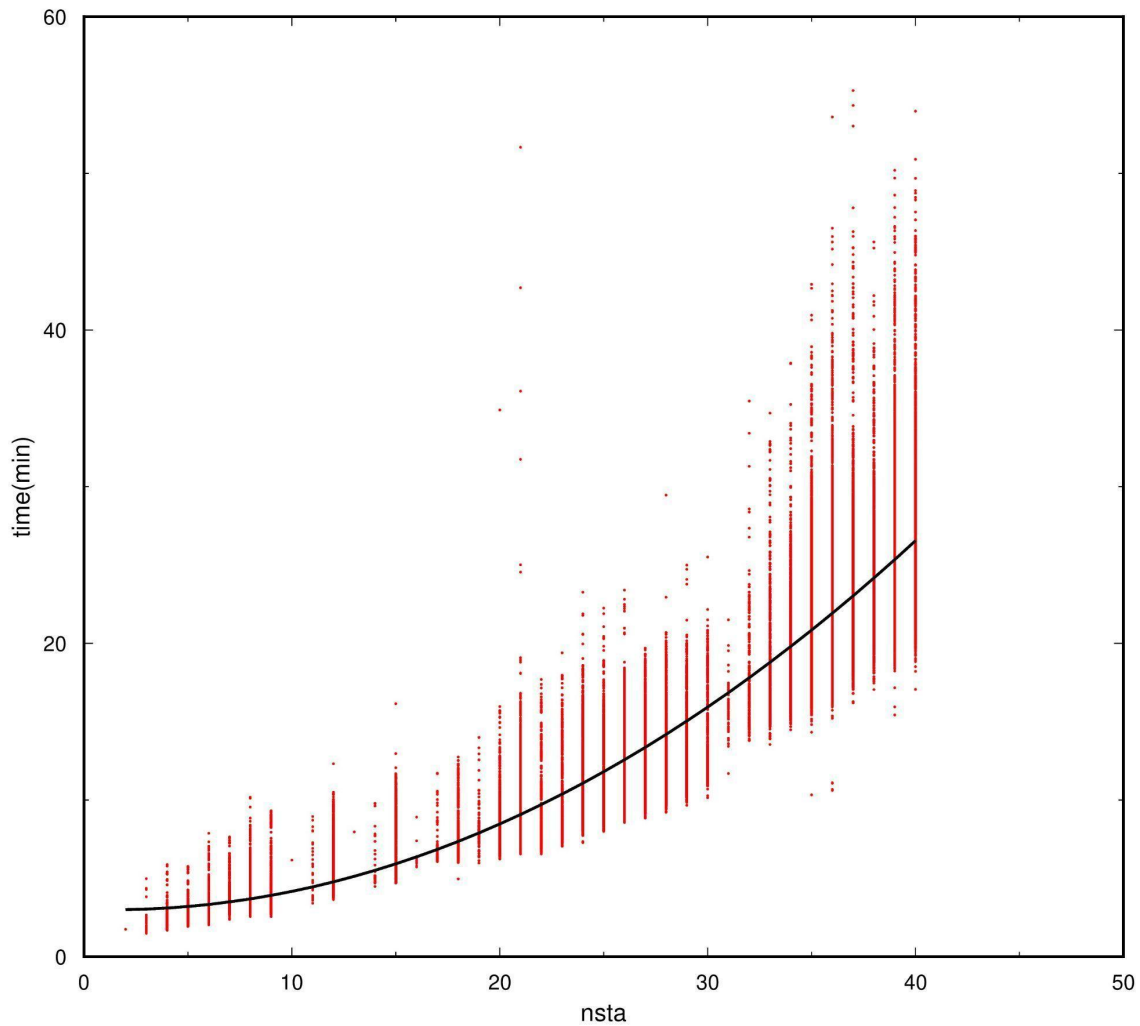
Fig. 6: Calculation time for GAMIT solutions using GALILEO100 cluster in function of the number of sites (nsta).

283

4 Geodetic time series and velocities dataset

This section considers the geodetic time series and velocity products provided. In support of the dataset, we illustrate several tests performed to check the reliability of the documented results. For the sake of simplicity, we define the results of this study as "final time series" and "final velocities", and those estimations retrieved from the tests as "test time series" or "test velocities" .

289 **4.1 Time series quality**

290 We illustrate here the GNSS time series resulting from the data processing as a whole, whereas time series for single stations

291 are provided in the dataset, as explained above.

292
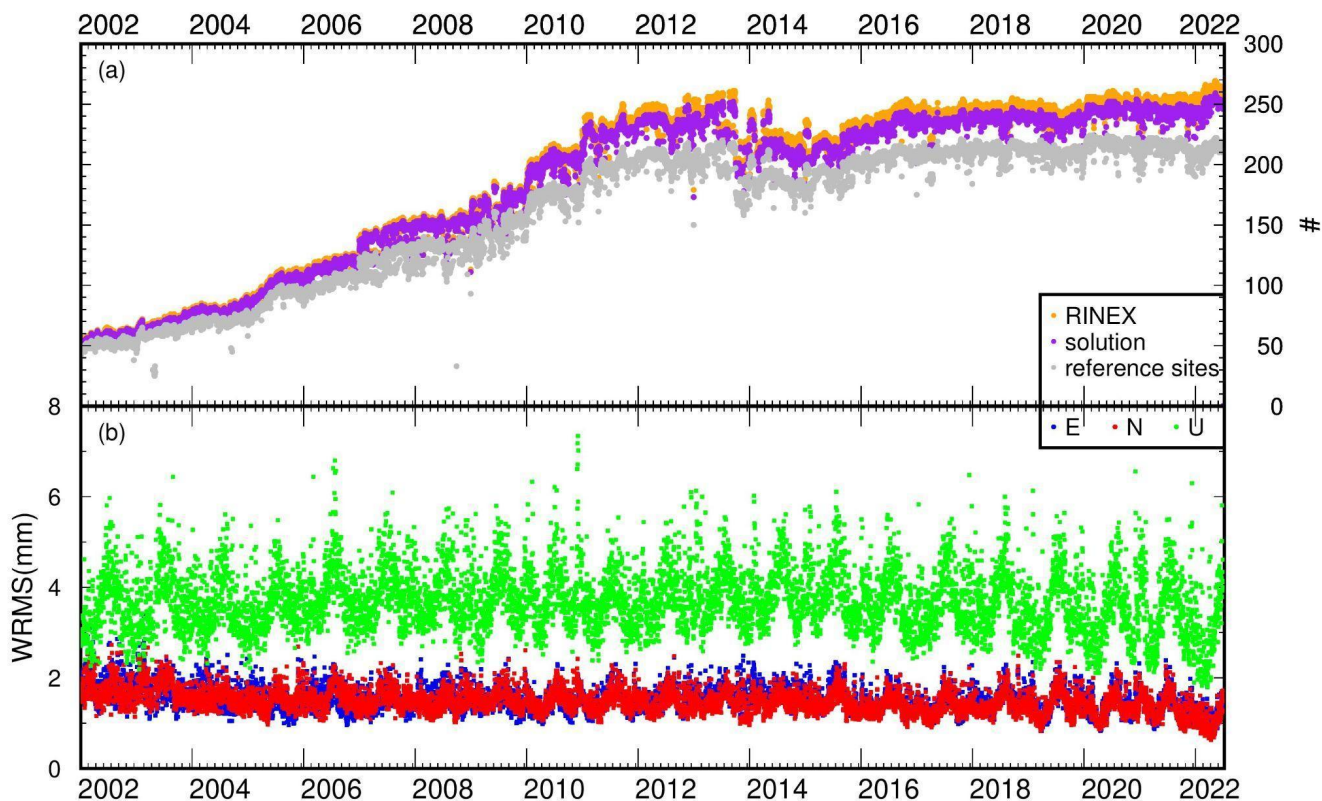
293 **Fig. 7: (a) Evolution of RINEX data available with time (orange dots), stations included in the solutions (purple dots) and stations**
294 **being used in the reference frame realisation (grey dots); (b) weighted root-mean-square (WRMS) scatter of the fits to the**
295 **coordinates of the reference frame stations in North (red), East (blue) and Up (green) components.**

296

297 The time series length and quality depend on the number of good observations recorded at the sites, which is reflected in the

298 number of solutions obtained for each station. Figure 7 shows the evolution of RINEX available with time, the sites included

299 in the solution, and those being used in the reference frame realisation, along with the weighted-root-mean-square (WRMS)

300 of the fits to reference frame stations. Through data processing, the recorded RINEX allowed obtaining almost 97,1% of

301 solutions (purple dots in Fig 7a), a percentage which is indicative of the goodness of the dataset and of the adoption of an

302 appropriate processing strategy. The percentage of missing solutions (~3%) are likely due to incomplete data records (RINEX

303 with less than 864 daily observations, i.e., with less than 30% of registrable daily observations) or bad data. As illustrated in

15

304   Section 3, in order to stabilise the solution we consider all stations with a random walk value lower than 0.5 mm^2/yr, which

305   led to consider as reference stations ~80% of the available stations after 2011, and even ~90 % or more in the first decade

306   (grey dots in Fig. 7a). The average WRMS fit to the reference frame stations (Fig. 7b) is 1.7, 1.8, and 4.2 mm in North, East,

307   and Up components, improving up to 20% in the latter since 2011, possibly thanks to the equipment improvements.

308   Figure 8 shows the stations' noise level through the representation of the WRMS of the time series and the RMS of the phase

309   residuals. Notably, the 90% of the stations show low noise levels, with values below 2 mm in the horizontal components and

310   below 4.1 mm in the vertical one.
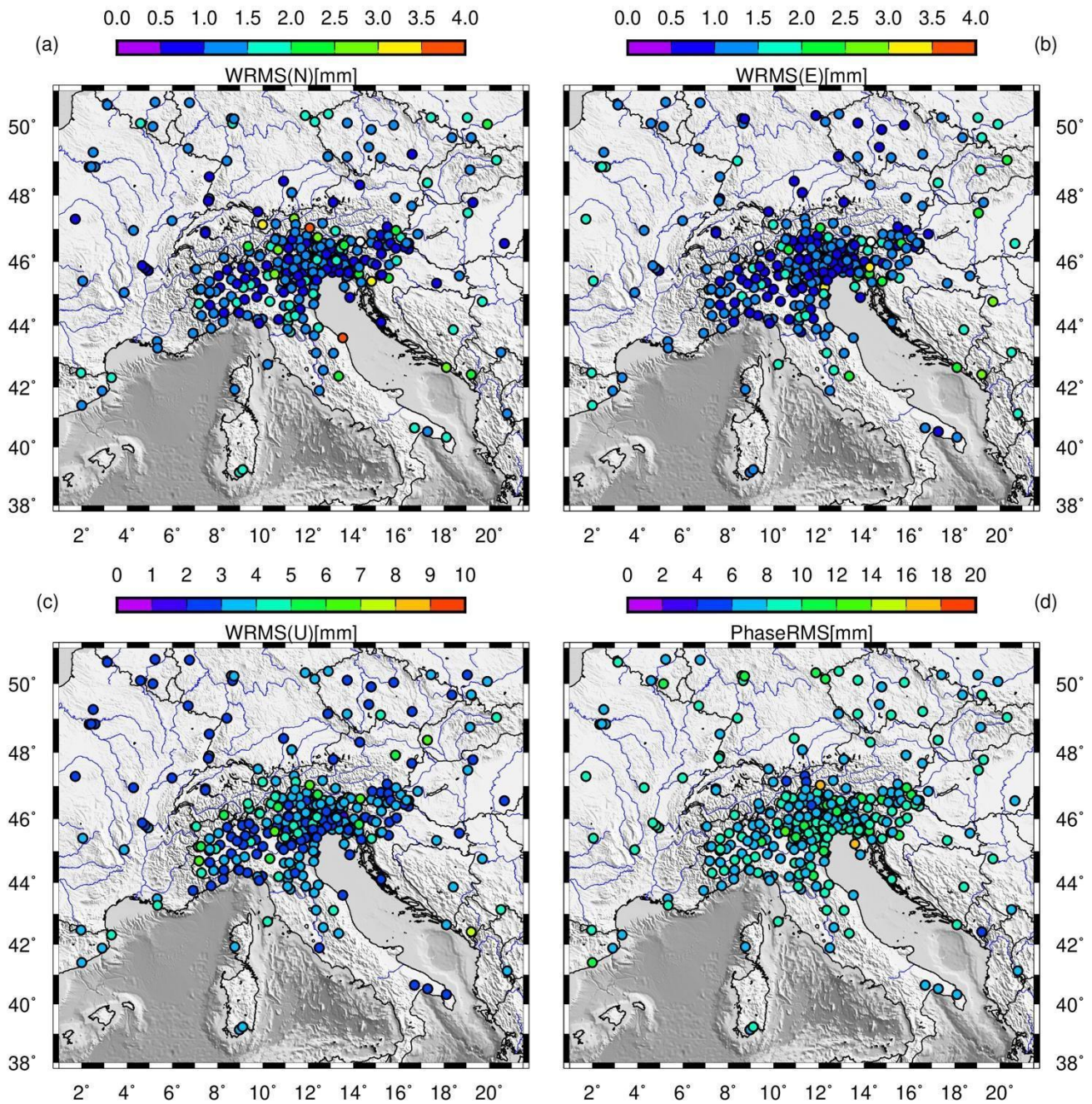
311

312 **Fig. 8: Time series WRMS in the horizontal (a, b) and vertical components (c) and time series RMS of the phase residuals (d).**

313

4.2 Geodetic velocities

The length of the time series is generally considered fundamental in determining the accuracy and precision of the estimated linear velocities. Blewitt and Lavallee (2002) show that a coordinate time series of 2.5 years is the minimum range to reduce velocity errors due to annual time series signals, caused primarily by surface loading due to hydrology and atmospheric pressure. However, the authors recommend using time series longer than 4.5 years to almost completely eliminate velocity biases. Data over a period less than 4.5 years are not suitable for studies requiring an accuracy of less than 1 mm/yr and the best results are obtained by using long time series (>8 years in length) which allow velocities to be estimated with an accuracy of 0.2 mm/yr in the horizontal components and 0.5 mm/year in the vertical component (Masson et al., 2019).
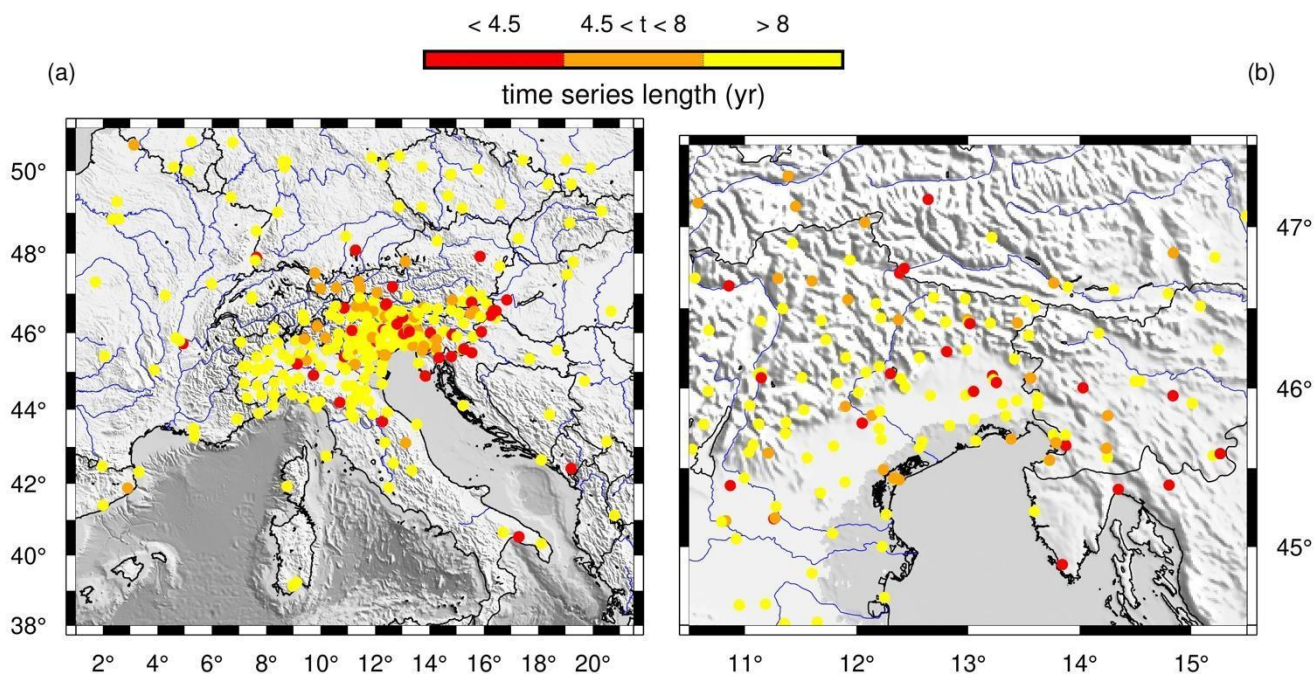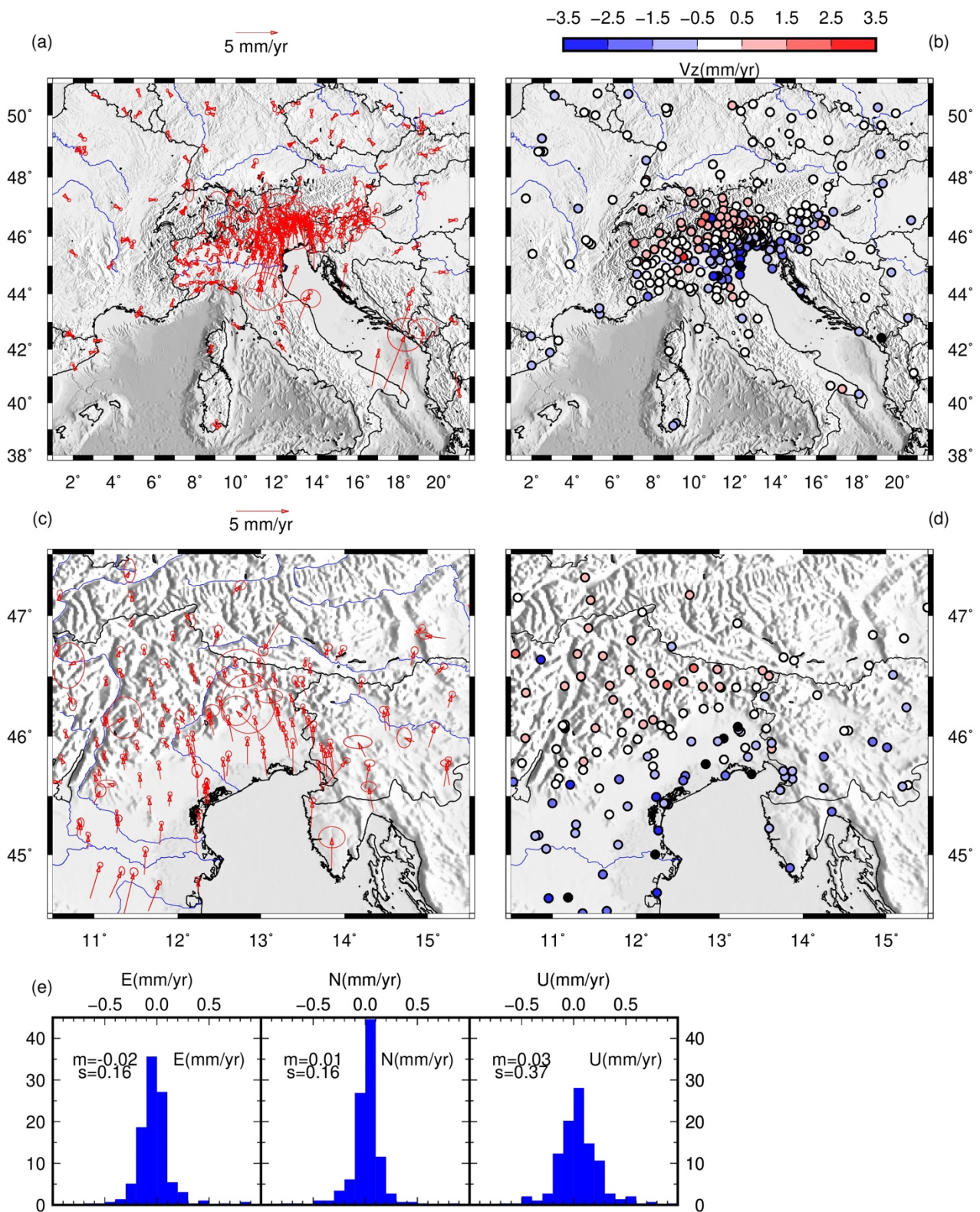

Fig. 9: Time series length of the stations considered in this study (a) with a zoom in the NE-Italy (b).

The stations considered in our study provide time series spanning from 0.27 (HELM) years to 20.49 years (among others, we cite AQUI, GENO, GRAZ, GSR1, and TORI), as shown in Fig. 9. Most of the sites provide time series longer than 4.5 years (84.4%), and even longer than 8 years length (69.4%), whereas just a small percentage are new stations providing coordinate time series shorter than one year (8.9%). However, newer stations are often located in proximity to older stations, thus allowing the retrieval of reliable and stable results also for that particular area (see Fig. 9b).

18

(a)

5 mm/yr

(b)

−3.5 −2.5 −1.5 −0.5 0.5 1.5 2.5 3.5

Vz(mm/yr)

(c)

5 mm/yr

(d)

(e)

E(mm/yr)

−0.5 0.0 0.5

m=−0.02
s=0.16

E(mm/yr)

N(mm/yr)

−0.5 0.0 0.5

m=0.01
s=0.16

N(mm/yr)

U(mm/yr)

−0.5 0.0 0.5

m=0.03
s=0.37

U(mm/yr)

332

Fig. 10: Estimated velocities with 95% confidence error ellipses, in the horizontal (a, c) and vertical components (vz) (b, d). (e) Histograms indicating the differences, along the three components, between velocity estimates calculated with GLOBK using the procedure described in Data Processing section, and those calculated using *tsfit* considering the stations with minimum 4.5 years long time series. Overall the differences are in a Gaussian shape, with mean and standard deviations values firmly below the mm/yr.

We estimated the velocities and uncertainties of all stations for the horizontal (Fig. 10a,c) and vertical components (Fig. 10b,d) using the GLOBK software. For completeness, we have also calculated the velocities using *tsfit*, a program that provides a linear fit of the time series, and we have compared the results (Fig. 10e) finding sub-millimeter differences. The estimated velocities in ETRF14 show the active deformation in the Adriatic side of the Central Apennines, in the few stations located in the SE-Italy (Puglia region) and in the NE-Italy, with horizontal displacement directed to the North-East with values of 2-3 mm/yr in the Apennines and also in the Friulian plain and coast. The NE-Italian Alps, instead, move with slower rates rounding 1 mm/yr. Significant horizontal motion is estimated in the SE-Italy, especially in the North velocity component, with 3.8 mm/yr and 4.2 mm/yr at USAL and MATE stations, respectively. The fastest motion (~ 7 mm/yr) is estimated at TARS and FATA stations (located close to each other and indistinguishable at the scale of Fig. 10). However, this value is not reliable because these stations provide less than 1-year of observations, as it can be inferred from the high uncertainty. The estimated vertical displacement highlights the subsidence in the Po Basin (up to 3.5 mm/yr) and the uplift in the mountains, more accentuated in the Eastern Alps than in the Apennines. Beside the European reference sites located beyond Italian territory, also the stations in the NW-Italy show no significant displacement. The single exception is LODI station, whose anomalous behaviour (~2 mm/yr velocity in the horizontal components and ~2.8 mm/yr of uplift) is due to its location on the top of a depleted methane reservoir, recently converted into an underground gas storage facility (Guidarelli et al., 2022). Zooming in the NE of the study area (Fig. 10c), a pattern of South-North decreasing velocities is distinguishable from the Friulian coastline and plain, to the Southern sector of the Eastern Alps, with an NNW orientation, whereas the stations located in Slovenia and Croatia show NNE oriented velocities. An anomalous south-directed motion is estimated in the OCHS station, in the Eastern Alps, likely due to a landslide motion occurring along the slope where the GNSS station is located.

5 Evaluation of the quality and robustness of the dataset

To evaluate the quality and robustness of the dataset, we perform some experiments with the processing procedure, analysed the quality of the stations, and compared our findings with previous studies.

5.1 Data processing tests

After determining time series, velocities and positions for each station, we test their stability and the reliability of the adopted processing procedure. For that, we perform a number of experiments on the available dataset to check for potential effects of selected options of the data processing with GAMIT/GLOBK (i.e., considering or avoiding tidal or non-tidal loadings or changing the reference stations) on the results. In this way, if these tests do not highlight significant differences with the study

results illustrated in the above sections, we can reasonably conclude that our results are reliable and not biassed by processing errors.

In one test, we change the model used to estimate the atmospheric delay. Instead of using the default Vienna Mapping Function numerical weather model (VMF1) calculated by TU Vienna by interpolating hydrostatic and wet mapping function coefficients as a function of time and location (Boehm et al., 2006a), we adopt the Global Mapping Function (GMF) model developed by Boehm et al. (2006b) which fits the European Centre for Medium-Range Weather Forecasts (ECMWF) data over 20 years. Then, since tides and non-tidal loadings are primary sources for time-variable displacements in station coordinates, we perform a test in which we consider the non-tidal atmospheric loading in the processing using a global gridded dataset provided by MIT. For both tests, we recalculate the time series and compare them to the original solution, finding no significant dissimilarity, with differences below 1 mm, in agreement with previous studies (Steigenberger et al., 2009; Labib et al., 2019)

Regarding the position time series and velocity estimations, we recall here that one delicate step in the procedure is knowing how to perform editing and weighting of the data, as well as the realisation of the reference frame.. To test these issues, we need to consider which stations to include explicitly, how to treat the orbits and the EOP, and practical constraints on computation speed and data storage. Although the GPS satellites provide a natural dynamic frame for ground-based geodesy, the doubly-differenced phase observations do not tie a ground station to the orbital constellation at the millimetre level. We define and realise a precise terrestrial reference frame by applying constraints to one or more sites in our network. To do that, we use the "generalised constraint" method of *glorg*, in which up to fourteen Helmert parameters (3 translations, 3 rotations, and 1 scale, and their rates) are estimated such that adjustments to *a priori* values of the coordinates of a group of stations are minimised. For continental-scale networks like the one considered in this study, we estimate translation and rotation and include as reference sites a set of distributed stations for which we have good *a priori* values and sound data.

Hence, we perform some tests to check the goodness of the stabilisation frame considered. We recalculate the time series by applying the translation-only transformation as in the EUREF standards (https://www.epncb.oma.be/_productsservices/analysiscentres/combsolframe.php), and find negligible differences in the time series. We then perform some tests for the first step of velocity estimation. First, we use as reference sites two different subsets of the reference sites set used in the final processing (see Test-1 and Test-2 in Fig. D1 in Appendix D). Second, on the second step of velocity estimation, we consider a regular grid of reference sites, generated considering a site every 2° (~ 222 km) (see Test-3 in Fig. D1 in Appendix D). Finally, we calculate the velocity field in our study area for each test. Overall, the mean difference values with respect to final velocities are very small, i.e. up to 0.02 mm/yr in the North, up to 0.06 mm/yr in the East and Up to 0.14 mm/yr in the vertical component.

Finally, we perform two last experiments to evaluate the effects on the velocity results of introducing the periodic term (annual signal) in the coordinate time series fitting and applying a less restrictive criterion for outliers, i.e., 5 sigmas instead of 3 sigmas. The mean differences, with respect to the final velocities, are of the order of 0.02 - 0.03 mm/yr in both cases for stations with at least 4.5 years of time series length.

399

5.2 Considerations on the stations quality

The alteration of the environmental conditions surrounding a GNSS station affects the RMS of the phase residuals. The environmental changes can be related not only to climatic conditions, e. g., an increase in the amount of weather perturbations due to the climate change, but also to urban developments in the proximity of the stations, manufact building, vegetation growth, radio-electronic sources perturbations, traffic increase, etc. In Fig. 11 we plot the RMS variation with time for some stations. A seasonal increase of the RMS is visible everywhere throughout the considered time interval.

406
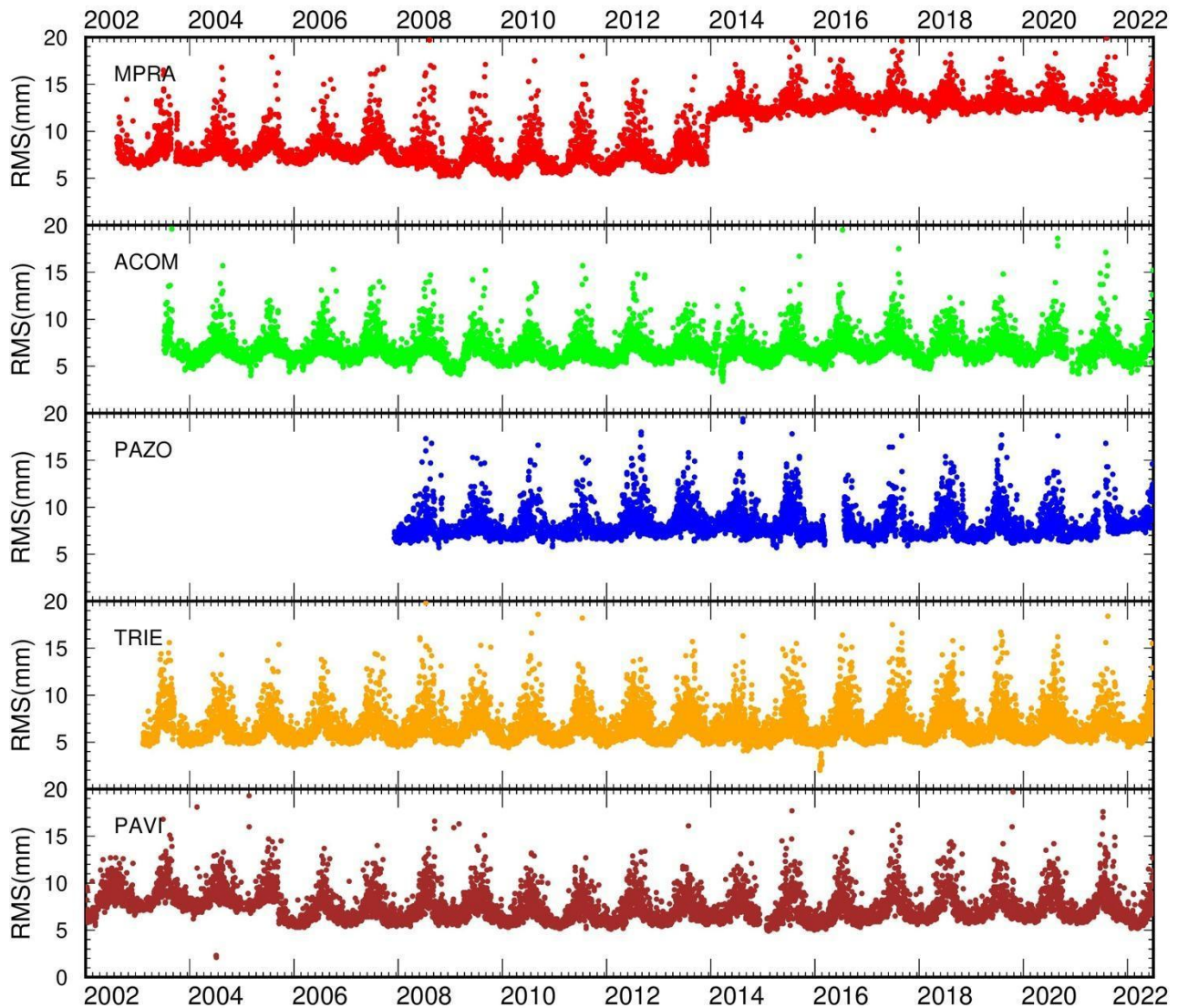
Fig. 11: Variation of the RMS of the phase residuals with time of different GNSS stations.

The phase RMS, typically 4-7 mm, increases up to 15-20 mm in July-August. This characteristic holds true for any station, whether it is located near the coast (i.e., TRIE), in the middle of the plain (as PAZO, PAVI) or in a mountain context (i.e., ACOM, located at 1774 m altitude; MPRA, located at 808 m altitude; ZOUF, located at 1946 m altitude). The same also occurs at the stations in northern Europe; thus, it is a characteristic independent of the geographic setting. A crosscheck on the sky plots shows that the phase RMS increases particularly during the daytime. We suspect it is due to a mismodeling of

23

the atmospheric delay. We certainly know that data coming from sites in the tropics are characterised by higher phase noise due to the higher water vapour content of the atmosphere. Orographic features such as mountain ranges are prone to produce a highly-turbulent and asymmetric atmosphere, which is particularly challenging to model. In other words, tropospheric asymmetries associated with topography, such as being on a mountain range's windward or leeward side, can produce asymmetrical time series scatter due to local-scale weather conditions (Materna, 2014).

Further considerations should be made for the MPRA station, which shows a systematic increase in the phase RMS since 2014. This condition is due to the construction of an electric tower in the proximity of the station, which has perturbed the site's noise level, leading to increased uncertainties, evident in the station time series (see Appendix A). Also PAVI station exhibits a systematically different RMS of the phase residuals since the second half of 2005, showing a decrease of ~ 2 mm. This decrease is likely due to a change in the equipment. The Trimble Zephyr Geodetic antenna (TRM41249.00), on day 14/09/2005 was substituted by a Leica choke ring antenna (LEIAT504) which features superior multipath rejection with uncompromised phase centre stability (<1mm) and is resistant to RF jamming (http://uec-sigmat.com/Leica%20AT504%20(GG)%20Choke%20Ring%20Antenna%20-%20gps_gnss.html#productCollateralTabs1).
However, the phase RMS decrease is not of such magnitude to be noticeable in the uncertainty level, or evident in the position time series of the site (see PAVI time series in the dataset).

Many authors have investigated the contribution of geodetic monuments to GNSS time series noise properties (e.g., Herring et al., 2016; Langbein and Svarc, 2019 and reference therein). However, our dataset mainly comprises stations installed on buildings, and each class of free-field installation (as defined in Fig. 5) consists of a limited number of stations. Therefore, inferring reliable conclusions about the different free-field installation types is impossible. In Fig. 12, we compared the noise properties of the time series (WRMS of the three components and HRW) of stations installed on buildings with those of free-field installations. We conclude that the stations on buildings are not significantly different from the stations installed on outcropping rocks.

437
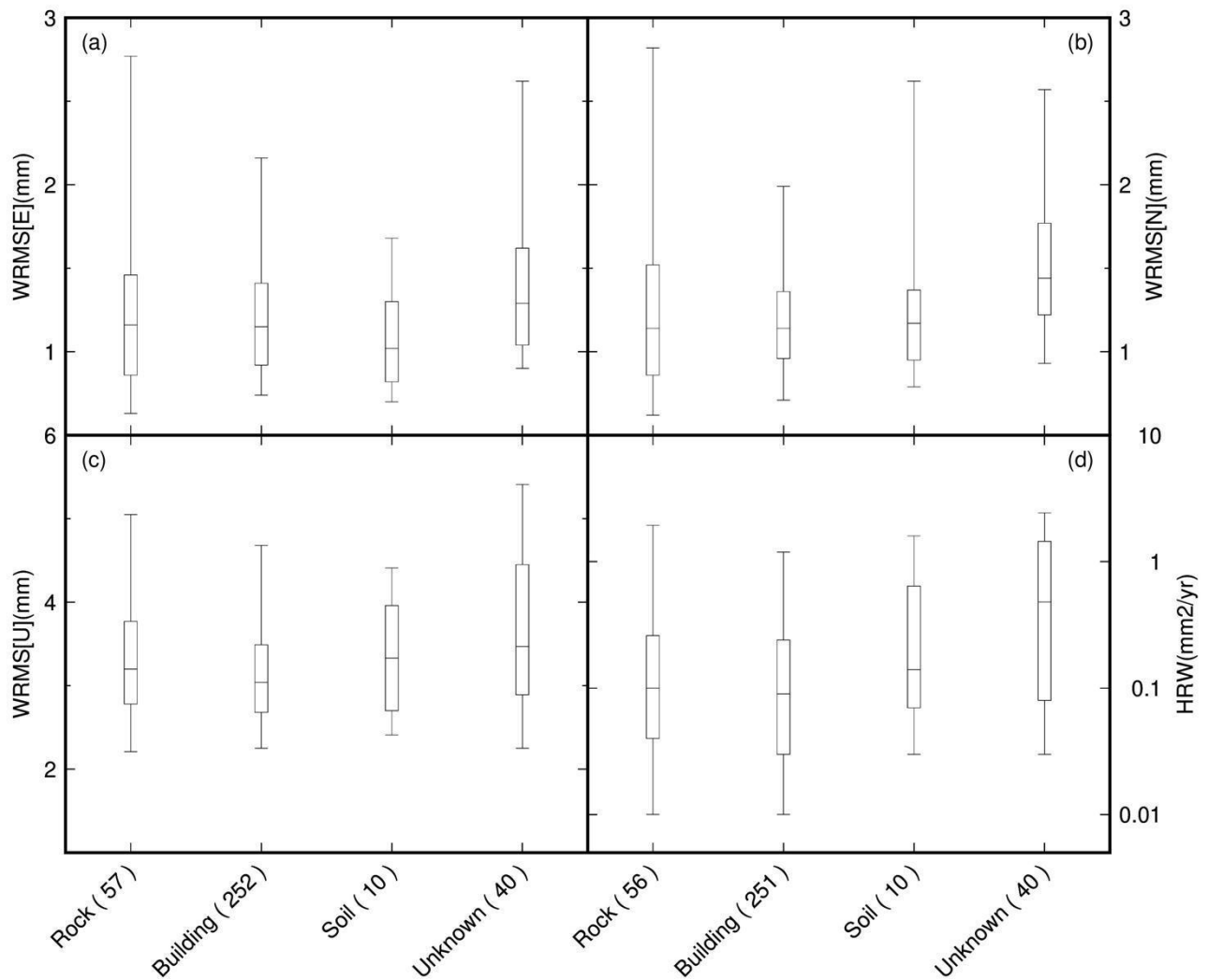
Fig. 12: Box-and-whisker plots showing the distribution of the weighted-root-mean-square (WRMS) values estimated from the scatter of the station time series residuals along the East (a), North (b) and Up (c) components, and the equivalent horizontal random walk (HRW) represented the time-correlated noise. The line in the centre of the box is the median value, the boxes encompass 50% of stations (25th to 75th percentiles), the whiskers encompass 90% of stations (5th to 95th percentiles).

442

5.3 Comparison with previous works

Different research groups published estimations of the velocity field in the area of interest of this study. Since the processing software or user-selected options can vary between different authors, through the comparison of our estimated velocities with those calculated by other researchers, we can evaluate the reliability of our solutions. If the misfits are not significant, we can

infer that our results are independent of data treatment and that our solutions are robust. On the contrary, if resulting velocities are inconsistent between different studies, this can likely be ascribable to the differences in the data treatment performed. It would be complicated to discriminate which research group has provided the best estimate of the velocity field.

We compared our results with those calculated by the Nevada Geodetic Laboratory (NGL), downloaded in the IGS14 reference frame from http://geodesy.unr.edu/ on 2023, 3rd March, and by Serpelloni and co-workers, which recently published the surface velocity of the Euro-Mediterranean region (Serpelloni et al., 2022). NGL uses the MIDAS software (Blewitt et al., 2016) to estimate the velocity field and automatically estimate the time series trend, identifying step discontinuities, outliers, seasonality and skewness in the data. Serpelloni and co-workers use the code of the Quasi Observation Combination Analysis (QOCA) software developed by JPL (https://qoca.jpl.nasa.gov) to analyse the time series and estimate the linear velocities. The comparison results are shown in Fig. 13 as histograms of solution differences. Overall, the mean differences are negligible, ranging from 0.01 mm/yr to 0.04 mm/yr in the horizontal component and to 0.01 mm/yr and 0.17 mm/yr in the vertical one, with the standard deviation ranging from 0.18 mm/yr to 0.47 mm/yr. Slightly greater values are found in the comparison with the NGL solution, especially in the Up component. These low discrepancies make us confident that our estimated velocities are robust and that the adopted data elaboration procedure is effective.

461
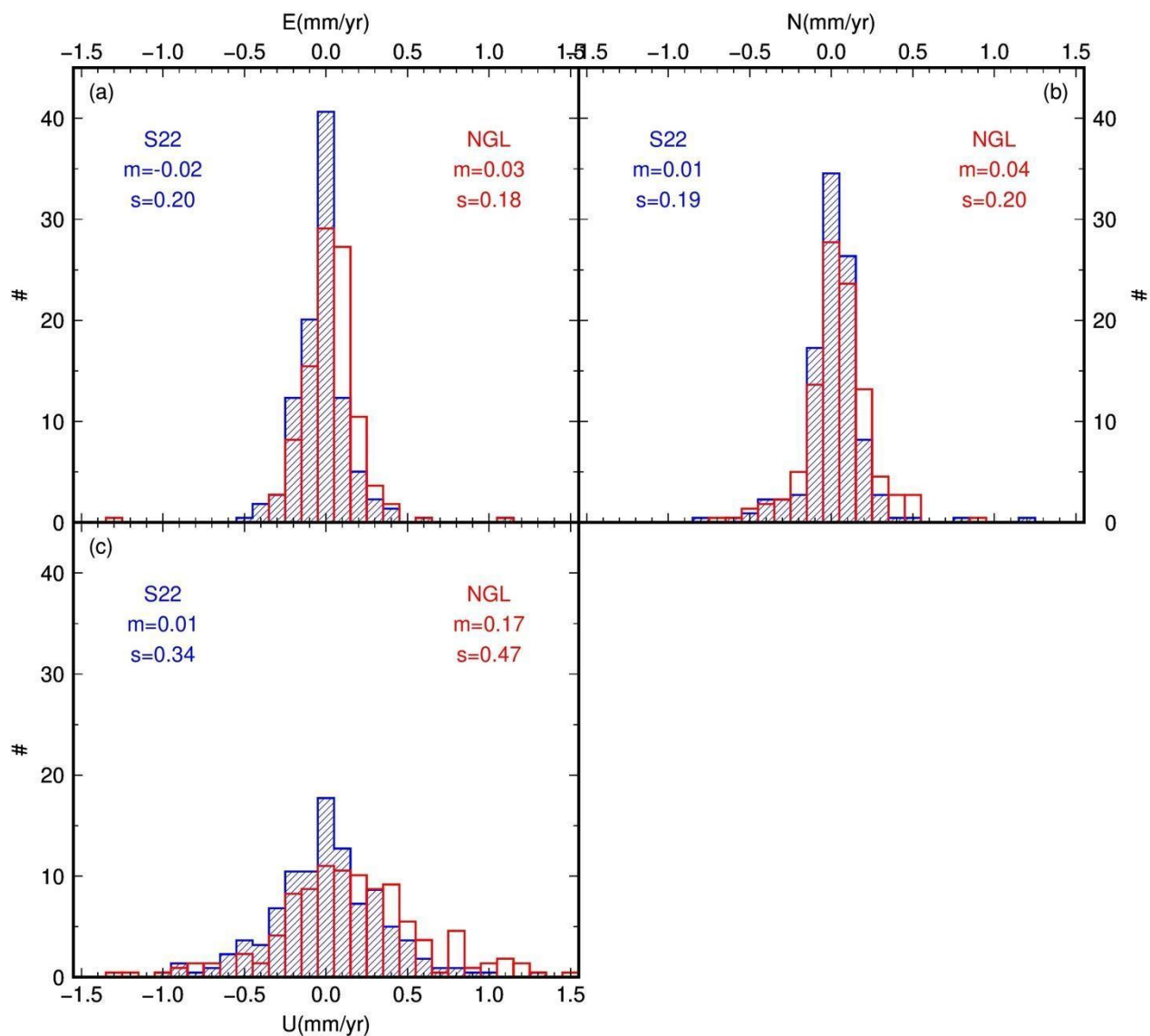
Fig. 13: Histograms of the differences between the velocity values estimated in this study, along the three components, and those estimated by Serpelloni and co-workers (S22, solution in blue colour) and by the Nevada Geodetic Lab (NGL, solution in red colour). Only the stations with a minimum of 4.5 years have been taken into consideration for the histograms.

465

6 Data availability

The geodetic time series and velocity dataset described in this article is accessible on Zenodo (https://doi.org/10.5281/zenodo.8055800, Tunini et al., 2024). The products are distributed under the Creative Common licence CC BY 4.0. The time series for each GNSS station, covering the 2002-2022 time interval (the last day processed is 2022, 30th June), are supplied in both international and Eurasia reference frames (ITRF14 and ETRF14). Besides the GNSS time series plots, GAMIT/GLOBK pos-formatted files and ASCII formatted (Solution INdependent Exchange - SINEX) daily files are provided. Velocity values are also provided in ITRF14 and ETRF reference frames, and made available through tables and ASCII-formatted SINEX files. An annual update of the estimated velocities is planned, while daily updated time series will be available via https://doi.org/10.6092/frednet (OGS, 2016) by clicking on the "solutions" link. Further related information regarding the present article (i.e., command files, information on jumps and discontinuities affecting the time series due to earthquakes or equipment changes, station information, etc.) is provided at the same link of the dataset (OGS, 2016).

7 Conclusions

This paper reports the processing of two decades of continuous GNSS observations focused on the slowly convergent margin between the Eurasia plate and the Adria microplate.

The dataset, available on Zenodo (https://doi.org/10.5281/zenodo.8055800, Tunini et al., 2024), contains the coordinate time series in both international and European reference frames, and velocity estimates for 350 permanent GNSS stations belonging to different regional and international networks, covering a time interval from 2002-01-01 to 2022-06-30. The time series are provided purged of undesirable values, removed according to the following criteria: (i) formal uncertainties; (ii) residuals concerning the RMS of the fit value and (iii) noise level. The estimated velocity values are retrieved from combining all the cleaned daily solutions.

Other research groups have also estimated consistent geodetic velocity values, but the corresponding time series are rarely retrievable. Therefore, the time series dataset presented here constitutes an important and complete source of information on the deformation of an active but slowly converging margin during the last two decades. In addition, the resulting time series are currently calculated and stored daily as part of a long-term monitoring project, and can be accessed at any time via https://doi.org/10.6092/frednet, while the velocity solutions will be updated annually. An overview of the input data used, GNSS stations information and data processing strategy is documented.

The original input data are RINEX-formatted daily GNSS observations, sampled every 30s and processed using the GAMIT/GLOBK software package version 10.71. Data processing was performed on the HPC cluster GALILEO100 from CINECA, which uses the SLURM system for job scheduling and workload management. Different experiments have been carried out on the same HPC cluster to evaluate the "goodness" of the applied processing procedure and the solidity of the solutions. The good results of the tests allow us to be confident that the dataset provided is accurate and robust, and it can be

498　　used for high-precision deformation studies. In future studies, data from other GNSS systems, such as Galileo or GLONASS

499　　observations, could also be included in the input data to provide further results and insights into the study region.

500

APPENDIX A. The OGS geodetic network: FReDNet

The Friuli Regional Deformation Network FReDNet (https://frednet.crs.ogs.it) is the OGS geodetic network established since the early 2000's in NE-Italy. Its primary objective is to monitor the distribution of crustal deformation and provide supplementary information for the regional earthquake hazard assessment (Zuliani et al., 2018). First stations of FReDNet were installed in 2002. Since then, FReDNet has grown until counting, nowadays, 22 permanent GNSS stations covering homogeneously the eastern Alps, the alluvial plain and the coastal areas of NE-Italy (Fig. 1). Most of the time series are longer than 15 years (Table A1).

Table A1. FReDNet stations specifics. MGBU station was installed on 2022, June 30th, therefore it is not included in the solution presented in the main text of the manuscript. UDIN is not operative anymore. H = hourly data sampled at 1s; D = daily data sampled at 30s; G = GLONASS satellites; R = RTK service; E = station belonging to EUREF Permanent Network (EPN) and data available from official EPN website https://www.epncb.oma.be/_networkdata/siteinfo4onestation.php?station=ZOUF00ITA. Rock = site installed on hard terrain (not soil) or outcropping rocks. Building = site installed on a building or similar manufacts, like a wall, both on roof or fixed to the side wall. Soil = site installed on a soft terrain. *station name under definition; **dismissed in 2006.

	GNSS station	Antenna	Receiver	Operative since	Available services	Monument type	Location
1	ACOM	ASH701945E_M	TPS NET-G5	2003	H, D, G, R	concrete pillar with steel rods	Rock
2	AFAL	ASH701945E_M	TPS GB-1000	2003	H, D, G, R	concrete pillar with steel rods	Rock
3	CANV	ASH701945E_M	TPS NET-G5	2004	H, D, G, R	concrete pillar with steel rods	Rock
5	CODR	ASH701945E_M	TPS NET-G3A	2007	H, D, G, R	steel mast	Building
6	FUSE	ASH701945E_M	TPS NET-G5	2007	H, D, G, R	concrete pillar with steel rods	Rock
7	JOAN	ASH701945E_M	TPS NET-G5	2007	H, D, G, R	concrete pillar with steel rods	Rock
8	LODI*	TPSCR.G5	TPS NET-G5	2017	H, D, G	miscellaneous	Soil

| 9	MDEA	ASH701945E_M	TPS NET-G5	2003	H, D, G, R	concrete pillar with steel rods	Rock
10	MGBU	TPSCR.G5	TPS NET-G5	2022	H, D, G, R	concrete pillar with steel rods	Rock
11	MPRA	ASH701945E_M	TPS NET-G5	2002	H, D, G, R	concrete pillar with steel rods	Rock
12	NOVE	TPSCR3_GGD	TPS GB-1000	2009	H, D, G, R	steel mast	Soil
13	PAZO	TPSCR.G3	TPS NET-G3A	2007	H, D, G, R	steel mast	Soil
14	PMNT	TPSCR.G5	TPS NET-G3A	2015	H, D, G, R	steel mast	Rock
15	SUSE	TPSCR.G3	TPS NET-G3A	2011	H, D, G, R	concrete pillar with steel rods	Soil
16	TOLS	TPSCR.G5	TPS GB-1000	2021	H, D, G, R	steel mast	Building
17	TRIE	ASH701945E_M	TPS NET-G5	2003	H, D, G, R	steel mast	Building
18	UDI1	ASH701945E_M	TPS NET-G3A	2006	H, D, G, R	steel mast	Building
19	UDI2	LEIAR20	LEICA GR25	2010	H, D, G, R	steel mast	Building
--	UDIN**	ASH701975.01AGP	ASHTECH UZ-12	2002	H, D	steel mast	Building
20	VALS	TPSCR.G5	TPS NET-G5	2021	H, D, G, R	steel mast	Rock
21	VARM	TPSCR.G5	TPS NET-G5	2012	H, D, G, R	steel mast	Rock
22	ZOUF	ASH701945C_M	TPS GB-1000	2002	H, D, R, G, E	concrete pillar with steel rods	Rock

516

517 As mentioned in the main text, data from FReDNet are collected, quality-checked, transformed into the RINEX-formatted
518 data, and then released under a Creative Common licence (CC BY), through a public ftp repository, as hourly and daily files
519 at both 1s and 30s sampling. The repository is the FReDNet Data Centre (OGS, 2016) accessible at the link
520 https://doi.org/10.6092/frednet, where also metadata of FReDNet sites (sitelogs in IGS format) are available. Pictures of
521 FReDNet stations are, instead, available on the FReDNet website https://frednet.crs.ogs.it. FReDNet provides real-time data
522 as well, through the Real Time Kinematics (RTK) services, which allow reaching a centimetre-level accuracy in the
523 positioning. The real-time data are available, free of charge, through the NTRIP (Networked Transport of RTCM via Internet
524 Protocol) distribution server.
525 Most of FReDNet stations are installed on solid rock or firmly monumented in the thick pebbly layer of the alluvial plain,
526 whereas 5 of them (CODR, TRIE, UDIN, UDI1, UDI2) are located on the roofs of small buildings. All the stations are
527 equipped with multi-frequencies and multi-constellations devices (Table A1). If the Topcon TPS GB-1000 and TPS NET-G3
528 receivers can track GPS and GLONASS satellite systems and just L1 and L2 frequency signals, the newest receivers TPS
529 NET-G5 are capable of tracking GPS, GLONASS, Galileo, and Beidou satellites and the signals L1, L2 and L5.
530 During the installation phase of FReDNet sites, particular attention had been paid to the site monument, which is crucial for
531 providing a stable and secure support for the antenna and hence for ensuring the good quality of the data retrieved. The
532 construction material should guarantee, within a reasonable low cost for building and maintenance, stability with time,
533 corrosion resistance, long term survivability, minimal interaction with signal, resistance to frost action and temperature
534 variations, and low or negligible amount of metal in the close proximity of the antenna. The site selected for placing the
535 monument should be easy accessible, clear of reflecting surfaces that can lead to multipath issues, with clear horizon and
536 controlled vegetation, and based on a shallow high quality bedrock with no local crust instabilities (cracks, cavities, etc.).
537 FReDNet sites were selected following the IGS recommendations, and periodically station maintenance is carried out to cut
538 grown vegetation in proximity of the station or to restore the data connection. However, sometimes the environment changes
539 with no possibility of restoring the initial conditions. One example is MPRA station. Though the initial location accomplished
540 all the IGS requirements (https://files.igs.org/pub/station/general/IGS%20Site%20Guidelines%20July%202015.pdf), in 2014
541 an electricity pylon was built in the proximity of the station, with consequences on the background noise level, as evidenced
542 by increased error bars in the coordinate time series and in the phase RMS time series (Fig. A1). Nonetheless, our data
543 processing strategy (illustrated in Section 3 of the main text) allows us to retrieve a stable solution, even with the presence
544 of noise time series as the one provided by MPRA station.

545
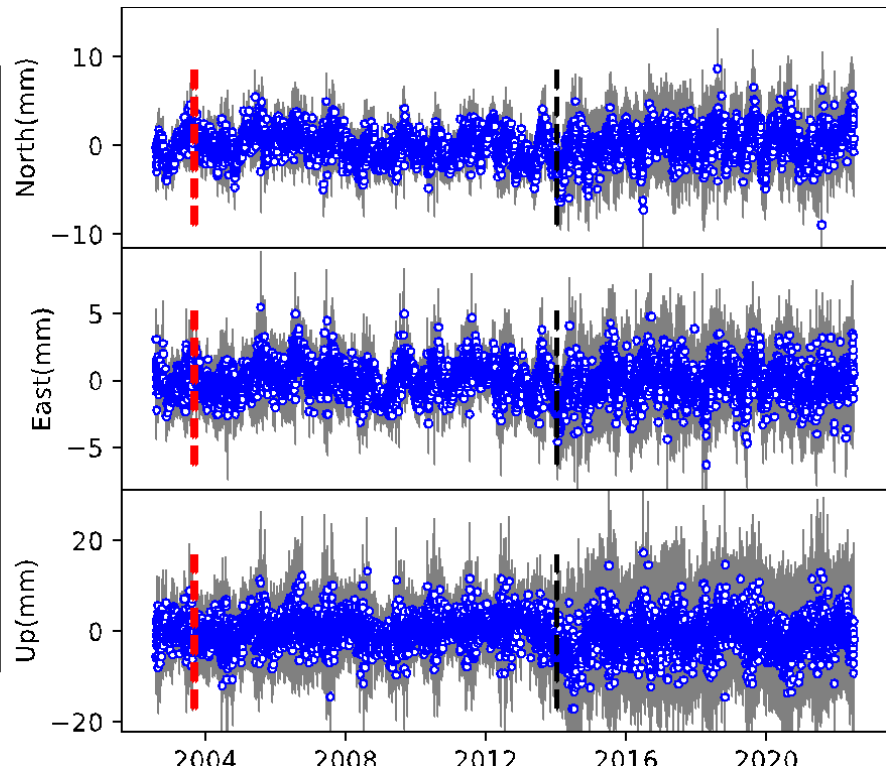
546
547 **Fig. A1: MPRA station photo and time series of the residuals. Red dashed line indicates a change of the antenna, while black**
548 **dashed line indicates the approximate date of the installation of the electricity pylon imaged in the photo.**
549

APPENDIX B. List of GNSS networks

Table B1. List of GNSS networks that we use to collect, archive and process daily RINEX data.

Network name	Data Provider	www and/or DOI
EPN (EUREF Permanent Network)	EUREF Consortium	http://www.epncb.oma.be/
EPOSA	Echtzeit Positionierung Austria	https://www.eposa.at/englisch
FReDNet (Friuli Regional Deformation Network)	National Institute of Oceanography and Applied Geophysics - OGS	http://frednet.crs.ogs.it/ and https://doi.org/10.6092/frednet
Marussi	FVG regional council	https://rem.regione.fvg.it
RING	National Institute of Geophysics and Volcanology (INGV)	http://ring.gm.ingv.it and https://doi.org/10.13127/ring
SIGN	Geodetic Institute of Slovenia	https://gu-signal.si
SLOV	University of Ljubljana and the non-profit organisation Zavod MPRI, raziskovalna in razvojna dejavnost	
SPIN	CSI-Piemonte	https://www.spingnss.it
STPOS	Provincia Autonoma di Bolzano	http://www.stpos.it/
TPOS	Provincia Autonoma di Trento	http://www.tpos.provincia.tn.it/
VNTO	Regione Veneto	http://retegnssveneto.cisas.unipd.it/
LIGU	Regione Liguria	https://geoportal.regione.liguria.it/servizi/rete-gnss-liguria.html/
ASI	Agenzia Spaziale Italiana	http://geodaf.mt.asi.it/

APPENDIX C. Daily local data processing

We implemented on a local machine the processing procedure described in the Section 3 of the main text with the aim to process the data following the 30th June of 2022. We have made the procedure automatic for daily processing. The local machine is a Mac mini equipped with Mac OS X (10.13) operative system. We use a crontab utility to manage the download of required input files, the update of metadata and the computation of daily solutions. From MIT, SOPAC, CDDIS and IGS repositories, we retrieve daily updates and files about orbits, atmospheric and tropospheric parameters, satellites aircrafts and ground station parameters, Earth orientation parameters, oceanic loading and tides, ionospheric and navigation files. RINEX files from FReDNet stations, EPOSA network and SLO_GPS stations are collected from OGS internal repositories. Observations from other networks are collected from the public data repositories of the networks, EPN data distribution services and EPOS service. Observations are downloaded on a daily basis, with a check for eventual missing observations in the 21 days before the processing date, in order to fix eventual data interruption or connectivity problems. Stations metadata are also downloaded periodically in the form of sitelogs from the public data repositories of the networks or from the M3G service and used to update the station information file and the file with the discontinuity.

The automated procedure provides two types of time series for each GNSS station: i) coordinate time series obtained using IGS final orbit files (more precise) and ii) coordinate time series obtained using IGS rapid orbit files, which are less precise but available with just 3 days latency (https://cddis.nasa.gov/Data_and_Derived_Products/GNSS/orbit_products.html). In particular, coordinate time series are calculated using final orbit files until 30 days before the processing date, and using rapid orbit files until 3 days before the processing date. An example of the resulting time series is given in Fig. C1.

Once the daily processing is finalized, an automatic e-mail message is sent to the data analysts with the summary of the processing results.

Finally, a periodic download of the latest tar-file containing incremental updates for GAMIT/GLOBK software is planned, in order to keep the software updated. We also plan to update the velocity solution each year.
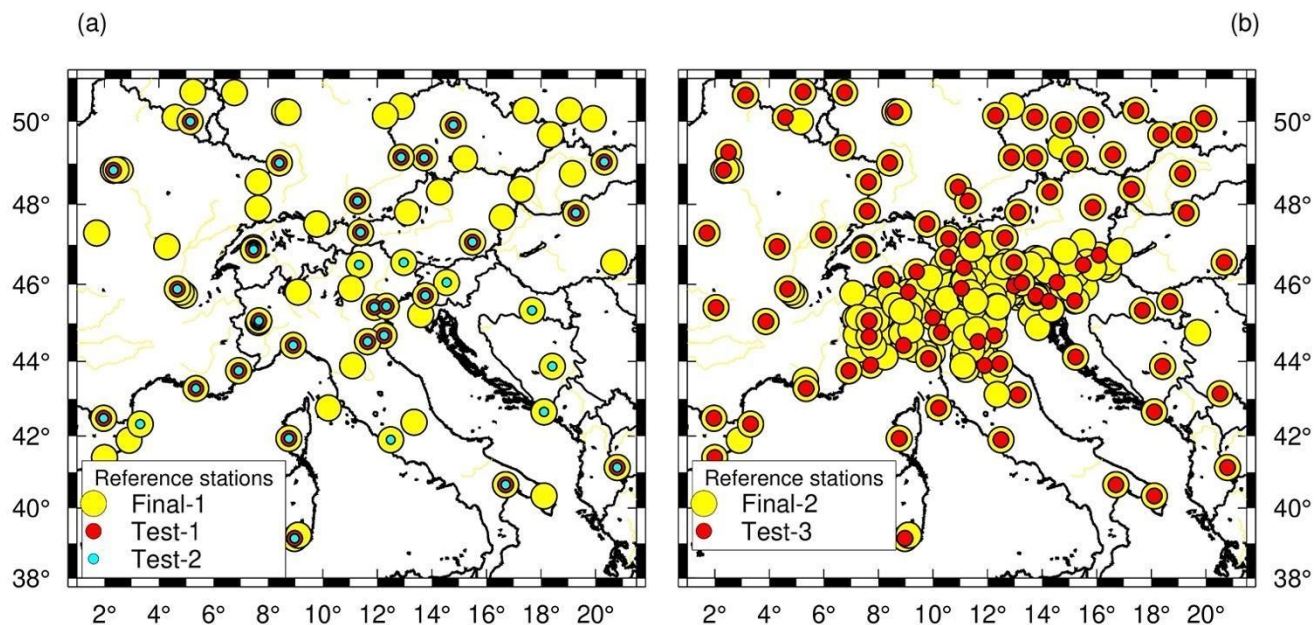
579
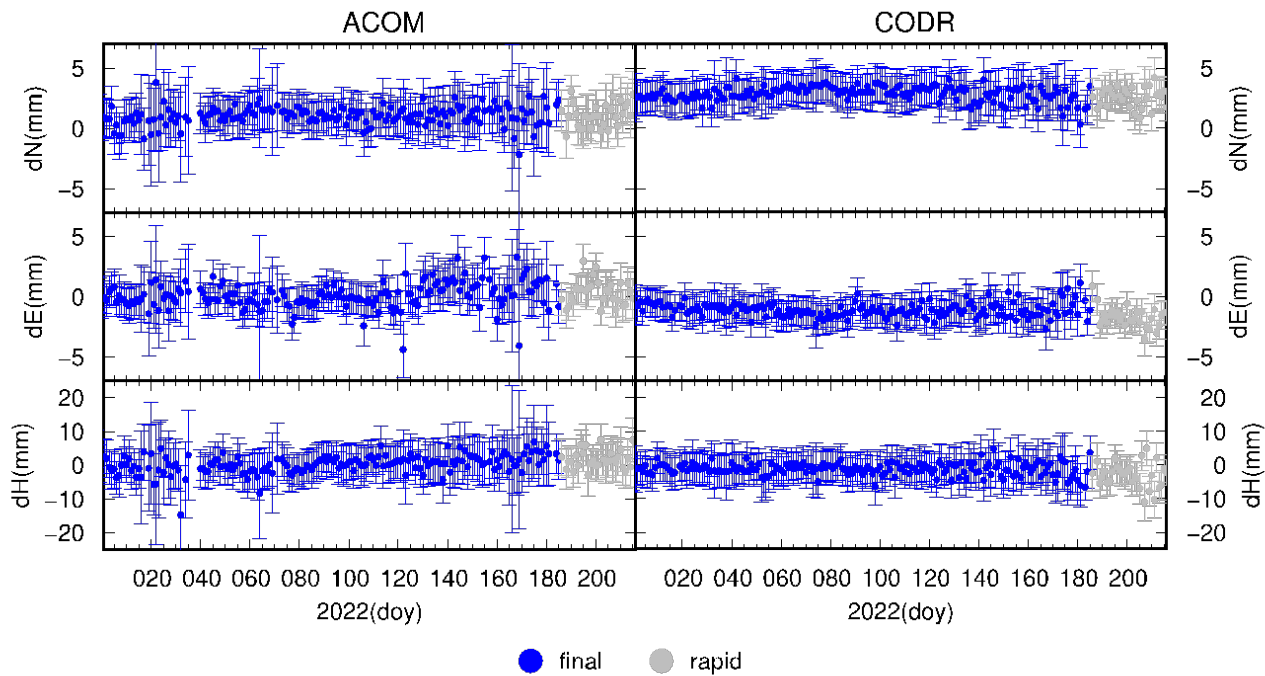
580 **Fig. C1: Coordinate time series in ETRF14 reference frame, calculated using final orbits (blue symbols) and rapid orbits (grey**
581 **symbols). Example for ACOM and CODR stations covering the time interval 2022-01-01/2022-08-04.**

582

583 **APPENDIX D. Reference sites**

584

585 **Fig. D1: Reference sites used in the tests (Test-1, Test-2, Test-3) illustrated in Section 5.1, plotted as red and cyan circles,**
586 **compared to the reference sites used in the final processing (Final-1 and Final-2 indicate the first and second iteration,**
587 **respectively, of the velocity calculation explained in Section 3), plotted as yellow circles.**
588

589 **Author contributions**

590 DZ, GR, AM, LT developed the concept of this work. DZ developed the FReDNet network with the contribution of OGS
591 technical staff, and he set up the real-time data distribution service. AM, LT processed and elaborated the dataset, and prepared
592 the manuscript and the figures. AM, LT, GR, DZ reviewed and edited the manuscript. All the authors have read and approved
593 the submitted manuscript.

594 **Competing interests**

595 The authors declare that they have no conflict of interest.

596 **Acknowledgements**

References

Alken, P., Thébault, E., Beggan, C.D. Amit, H, Aubert, J., Baerenzung, J., Bondar, T.N., Browin, W.J., Califf, S., Chambodut, A., Chulliat, A., Cox, G.A., Finlay, C.C., Fournier, A., Gillet, N., Grayver, A., Hammer, M.D., Holschneider, M., Huder, L., Hulot, G., Jager, T., Kloss, C., Korte, M., Kuanh, W., Kuvshinov, A., Langlais, B., Léger, J.-M., Levur, V., Livermore, P.W., Lowes, F.J., Macmillan, S., Magnes, W., Mandea, M., Marsal., S., Matzka, J., Metman, M.C., Minami, T., Morschhauser, A., Mound, J.E., Nair, M., Nakano, S., Olsen, N., Pavón-Carrasco, F.J., Petrov, V.G., Ropp, G., Rother, M., Sabaka, T.J., Sanchez, S., Saturnino, D., Schnepf, N.R., Shen, X., Stolle, C., Tangborn, A., Tøffner-Clausen, L., Tob, H., Torta, J.M., Varner, J., Vervelidou, F., Vigneron, P., Wardinski, I., Wicht, J., Woods, A., Yang, Y., Zeren, Z., and Zhou, B.: : International Geomagnetic Reference Field: the thirteenth generation. Earth Planets Space 73, 49, doi: 10.1186/s40623-020-01288-x, 2021.

Altamimi, Z., Rebischung, P., Metivier, L., and Collilieux, X.: ITRF2014: A new release of the International Terrestrial Reference Frame modeling nonlinear station motions, J. Geophys. Res. Solid Earth, 121, doi:10.1002/2016JB013098, 2016.

Altamimi, Z., Métivier, L., Rebischung, P., Rouby, H., Collilieux, X.: ITRF2014 plate motion model, Geophysical Journal International, 209(3),1906–1912, doi:10.1093/gji/ggx136, 2017.

Amante, C., and Eakins, B. W. (2009). ETOPO1 1 Arc-Minute Global Relief Model: Procedures, Data Sources and Analysis. NOAA Technical Memorandum NESDIS NGDC-24. Silver Spring: NOAA.

Battaglia, M., Zuliani, D., Pascutti, D., Michelini, A., Marson, I., Murray, M.H., Burgmann, R.: Network Assesses Earthquake Potential in Italy's Southern Alps, EOS, 84, 262–264, 2003.

631

632 Blewitt, G, and Lavallee, D.: Effect of annual signals on geodetic velocity, J. Geophys. Res., 107 (B7), 2002.

633

634 Blewitt, G., Kreemer, C., Hammond, W.C., and Gazeaux J.: MIDAS robust trend estimator for accurate GPS station velocities

635 without step detection, Journal of Geophysical Research, 121, doi:10.1002/2015JB012552, 2016.

636

637 Blewitt, G., W. C. Hammond, and C. Kreemer: Harnessing the GPS data explosion for interdisciplinary science, Eos, 99,

638 https://doi.org/10.1029/2018EO104623, 2018.

639

640 Boehm, J., Werl, B., and Schuh, H.: Troposphere mapping functions for GPS and very long baseline interferometry from

641 European Centre for Medium-Range Weather Forecasts operational analysis data. doi:10.1029/2005JB003629, 2006a.

642

643 Boehm, J., Niell, A., Tregoning, P., and Schuh, H.: Global mapping function (GMF): a new empirical mapping function based

644 on numerical weather model data Geophys. Res. Lett. 33, 2006b.

645

646 Bragato, P. L., Comelli, P., Sara., A., Zuliani, D., Moratto, L., Poggi, V., Rossi, G., Scaini, C., Sugan, M., Barnaba C.,

647 Bernardi, P., Bertoni, M., Bressan, G., Compagno, A., Del Negro, E., Di Bartolomeo, P., Fabris, P., Garbin, M., Grossi, M.

648 Magrin, A., Magrin, E., Pesaresi, D., Petrovic, B., Plasencia Linares, M.P., Romanelli, M., Snidarcig, A., Tunini, L., Urban,

649 S., Venturini, E., Parolai, S.: The OGS - Northeastern Italy seismic and deformation network: Current status and outlook,

650 Seismol. Res. Lett. 92, no. 3, 1704–1716, doi:10.1785/0220200372, 2021.

651

652 Braitenberg, C., and Zadro, M.: The Grotta Gigante horizontal pendulums - instrumentation and observations. Bollettino di

653 Geofisica Teorica e Applicata, 40(3/4), 577–582, 1999.

654

655 Brancolini, G., Civile, D., Donda, F., Tosi, L., Zecchin, M., Volpi, V., Rossi, G., Sandron, D., Ferrante, G.M., and Forlin, E.:

656 New insights on the Adria plate geodynamics from the northern Adriatic perspective, Marine and Petroleum Geology, 109,

657 687-697, 2019.

658

659 Bressan, G., Barnaba, C., Peresan, A., & Rossi, G. Anatomy of seismicity clustering from parametric space-time analysis.

660 Physics of the Earth and Planetary Interiors, 320, 106787, 2021.

661

662 Castellarin, A., & Cantelli, L.: Neo-Alpine evolution of the southern Eastern Alps. Journal of Geodynamics, 30(1-2), 251-

663 274, 2000.

664

665   D'Agostino, N., Avallone, A., Cheloni, D., D'Anastasio, E., Mantenuto, S., and Selvaggi, G.: Active tectonics of the Adriatic
666   region from GPS and earthquake slip vectors. J. Geophys. Res. 113:B12413. doi: 10.1029/2008JB005860, 2008.
667

668   D'Agostino, N., Cheloni, D., Mantenuto, S., Selvaggi, G., Michelini, A., and Zuliani, D.: Strain accumulation in the southern
669   Alps (NE Italy) and deformation at the northeastern boundary of Adria observed by CGPS measurements. Geophys. Res.
670   Lett. 32:L19306. doi:10.1029/2005GL024266, 2005.
671

672   Devoti, R., Esposito, A., Pietrantonio, G., Pisani, A. R., and Riguzzi, F.: Evidence of large scale deformation patterns from
673   GPS data in the Italian subduction boundary. Earth and Planetary Science Letters, 311(3-4), 230-241, 2011.
674

675   Dong, D., Herring, T. A., and King, R. W.: Estimating Regional Deformation from a Combination of Space and Terrestrial
676   Geodetic Data. J. Geodesy 72 (4), 200–214. doi:10.1007/s001900050161, 1998.
677

678   Estey, L.H. and Meertens, C.M.: TEQC: The Multi-Purpose Toolkit for GPS/GLONASS Data and GPS Solutions; John Wiley
679   & Sons: New York, NY, USA, Volume 3, pp. 42–49, 1999.
680

681   Floyd, M. A., and Herring, T. A.: Fast statistical approaches to geodetic time series analysis. In J. P. Montillet & M. Bos
682   (Eds.), Geodetic Time Series Analysis in Earth Sciences Bos and Montillet, Springer Geophysics. Cham: Springer.
683   doi:10.1007/978-3-030-21718-1, 2019.
684

685   Floyd, M. A., Billiris, H., Paradissis, D., Veis, G., Avallone, A., Briole, P., McClusky, S., Nocquet, J.M., Palamartchouk, K.,
686   Parsons, B., and England, P. C.: A new velocity field for Greece: Implications for the kinematics and dynamics of the Aegean,
687   J. Geophys. Res., 115, B10403, doi:10.1029/2009JB007040, 2010.
688

689   Gerhard, W., Andreas, B., Martin, S.: RTK Networks based on Geo++ ® GNSMART—Concepts, Implementation, Results.
690   In Proceedings of the International Technical Meeting (ION GPS−01), Salt Lake City, UT, USA, 11–14 September 2001.
691

692   Guidarelli, M., Lanari, R. Bonano, M., De Luca, C., Magrin, A., Moratto, L., Peruzza, L., Romanelli, M., Romano, M. A.,
693   Sandron, D., Santulin, M., Tunini, L., Zeni, G., Zinno, I., Zuliani, D.: Concessione di stoccaggio di gas naturale "Cornegliano
694   Stoccaggio". Monitoraggio sismico e delle deformazioni superficiali. Anno di esercizio 2022 – Relazione semestrale. Rel.
695   OGS 2023/7 Sez. CRS 1, https://hdl.handle.net/20.500.14083/15762, 2022.
696

Herring, T. A., Melbourne, T. I., Murray, M. H., Floyd, M. A., Szeliga, W. M., King, R. W., ... & Wang, L.: Plate Boundary Observatory and related networks: GPS data analysis methods and geodetic products, Reviews of Geophysics, 54(4), 759-808, 2016.

Herring, T.A., King, R.W., Floyd, M.A., and McClusky, S.C.: Introduction to GAMIT/GLOBK Introduction to GAMIT/GLOBK, Release 10.7. Available at: http://geoweb.mit.edu/gg/docs/Intro_GG.pdf, 2018.

Hunter, J. D. : Matplotlib: A 2D Graphics Environment, Computing in Science & Engineering, vol. 9, no. 3, pp. 90-95, 2007.

Johnston, G., Riddell, A., Hausler, G.: The International GNSS Service. Teunissen, Peter J.G., & Montenbruck, O. (Eds.), Springer Handbook of Global Navigation Satellite Systems (1st ed., pp. 967-982). Cham, Switzerland: Springer International Publishing. DOI: 10.1007/978-3-319-42928-1, 2017.

Labib, B., Yan, J., Barriot, J. P., Zhang, F., & Feng, P.: Monitoring Zenithal Total Delays over the three different climatic zones from IGS GPS final products: A comparison between the use of the VMF1 and GMF mapping functions. Geodesy and Geodynamics, 10(2), 93-99, 2019.

Langbein, J., and Svarc, J. L.: Evaluation of temporally correlated noise in Global Navigation Satellite System time series: Geodetic monument performance. Journal of Geophysical Research: Solid Earth, 124(1), 925-942, 2019.

Lyard, F., Lefevre, F., Letellier, T., & Francis, O.: Modelling the global ocean tides: modern insights from FES2004. Ocean dynamics, 56, 394-415, 2006.

Magrin, A., and Rossi, G.: Deriving a new crustal model of Northern Adria: The Northern Adria Crust (NAC) Model. Frontiers of Earth Science, 8, doi:10.3389/feart.2020.00089, 2020.

Masson, C., Mazzotti, S., Vernant, P.: Precision of continuous GPS velocities from statistical analysis of synthetic time series, Solid Earth, 10: 329–342, https://doi.org/10.5194/se-10-329-2019, 2019.

Materna, K.: Analysis of atmospheric delays and asymmetric positioning errors in the global positioning system (Doctoral dissertation, Massachusetts Institute of Technology), 2014.

Matthews, K. J., Maloney, K. T., Zahirovic, S., Williams, S. E., Seton, M., and Müller, R. D.: Global plate boundary evolution and kinematics since the late Paleozoic: Global and Planetary Change, doi:10.1016/j.gloplacha.2016.10.002, 2016.

731

732 Noll, C.: The Crustal Dynamics Data Information System: A resource to support scientific analysis using space geodesy,
733 Advances in Space Research,Volume 45, Issue 12, 15 June 2010, Pages 1421-1440, ISSN 0273-1177, DOI:
734 10.1016/j.asr.2010.01.018, 2010.

735

736 OGS-Istituto Nazionale Di Oceanografia E Geofisica Sperimentale: Friuli Regional Deformation Network Data Center (1.0),
737 https://doi.org/10.6092/frednet, 2016.

738

739 Petit, G. and Luzum, B.: IERS conventions, Tech. rep., Bureau International des Poids et mesures sevres (France), 2010.

740

741 Priolo, E., Zinno, I., Guidarelli, M., Romanelli, M., Lanari, R., Sandron, D., Garbin, M., Peruzza, L., Romano, A., Zuliani,
742 D., Tunini, L., Magrin, A: The birth of an underground gas storage in a depleted gas reservoir - Results from integrated
743 seismic and ground deformation monitoring, under review.

744

745 Rossi, G., Pastorutti, A., Nagy, I., Braitenberg, C., and Parolai, S.: Recurrence of Fault Valve Behavior in a Continental
746 Collision Area: Evidence From Tilt/Strain Measurements in Northern Adria, Frontiers in Earth Science, 9, 641416, 2021.

747

748 Serpelloni, E., Anzidei, M., Baldi, P., Casula, G., and Galvani, A.: Crustal velocity and strain-rate fields in Italy and
749 surrounding regions: new results from the analysis of permanent and non-permanent GPS networks, Geophys. J. Int. 161,
750 861–880, doi: 10.1111/j.1365-246X.2005.02618.x, 2005.

751

752 Serpelloni, E., Cavaliere, A., Martelli, L., Pintori, F., Anderlini, L., Borghi, A., Randazzo, D., Bruni, S., Devoti, R., Perfetti,
753 P., and Cacciaguerra, S.: Surface Velocities and Strain-Rates in the Euro-Mediterranean Region From Massive GPS Data
754 Processing, Front. Earth Sci., 10, 1–22, 2022.

755

756 Steigenberger, P., Boehm, J., & Tesmer, V.: Comparison of GMF/GPT with VMF1/ECMWF and implications for
757 atmospheric loading. Journal of Geodesy, 83, 943-951, 2009.

758

759 Tunini, L., Magrin, A., Rossi, G., and Zuliani, D.: 2022.OGS.GPS.solution: GNSS time series and velocities about a slow
760 convergent margin processed on HPC clusters: products and robustness evaluation, https://doi.org/10.5281/zenodo.8055800,
761 2024.

762 U.S.G.S., US Geological Survey, Earthquake Hazards Program: Advanced National Seismic System (ANSS) Comprehensive
763 Catalog of Earthquake Events and Products: Various, https://doi.org/10.5066/F7MS3QZH, 2017.

764

765   Weber, J., Vrabec, M., Pavlovčič-Prešeren, P., Dixon, T., Jiang, Y., and Stopar, B.: GPS-derived motion of the Adriatic

766   microplate from Istria Peninsula and Po Plain sites, and geodynamic implications. Tectonophysics, 483(3-4), 214-222, 2010.

767

768   Wessel, P., Luis, J. F., Uieda, L., Scharroo, R., Wobbe, F., Smith, W. H. F., & Tian, D.: The Generic Mapping Tools version

769   6. Geochemistry, Geophysics, Geosystems, 20, 5556–5564. https://doi.org/10.1029/2019GC008515, 2019.

770

771   Zuliani, D., Fabris, P., Rossi, G.: FReDNet: Evolution of permanent GNSS receiver system. In: New Advanced GNSS and

772   3D Spatial Techniques Applications to Civil and Environmental Engineering, Geophysics, Architecture, Archeology and

773   Cultural Heritage, Lecture Notes in Geoinformation and Cartography; Cefalo, R., Zielinski, J., Barbarella, M., Eds.; Springer:

774   Cham, Switzerland, pp.123–137, 2018.